SSRG International Journal of Electrical and Electronics Engineering
ISSN: 2348-8379/ https://doi.org/10.14445/23488379/IJEEE-V13I3P114

Volume 13 Issue 3, 178-199, March 2026

Original Article

ANN-Controlled Z-Source Inverter Integrated Wind Energy System with DSTATCOM for Grid Support and Power Quality Improvement

Rajesh K[1*], Suresh Babu Daram[1]

[1*]*Department of Electrical and Electronics Engineering, School of Engineering,*
Mohan Babu University (Erstwhile Sree Vidyanikethan Engineering College), Tirupati, Andra Pradesh, India.

**Corresponding Author : 22201R020009@mbu.asia*

Received: 11 December 2025 Revised: 12 January 2026 Accepted: 20 February 2026 Published: 31 March 2026

Abstract *- This paper presents a grid-integrated wind energy system designed to enhance the reliability of electrical power supply to consumers while reducing dependence on the conventional distribution grid. In this system, an AC output from a Permanent Magnet Synchronous Generator (PMSG) is rectified and fed to a Z-source inverter for connection to the grid. The Z-source inverter performs the function of boosting the DC link voltage while converting it to AC power in one step, and therefore, it has been shown to reduce the overall size, cost, and voltage ripples of the system. A control strategy is developed to regulate the DC link voltage across the inverter bridge terminals, to maximize the power extracted from the wind turbine based on the Perturb and Observe (P&O) MPPT tracking method, and to ensure a unity power factor. The proposed control strategy utilizes two independent control variables, i.e., the shoot-through duty cycle and the modulation index, to separate DC side and AC side control. For addressing issues associated with weak grids, such as voltage fluctuations, harmonic distortion, and reactive power imbalance, a Distribution Static Compensator (DSTATCOM) is used. An adaptive Artificial Neural Network (ANN)-based control strategy is utilized to improve the performance of both the Z-source inverter and the DSTATCOM used in the hybrid renewable energy system proposed in this work. The ANN-based control strategy is able to mitigate transient disturbances, improve dynamic responses, and provide smart reactive power compensation under nonlinear and time-varying loading conditions. Compared to the traditional Proportional–Integral (PI) controller, the ANN-based controller has a fast response time, high adaptability, and high accuracy for improving the quality of power. Simulation results obtained from using MATLAB/Simulink show that the ANN-based controlled system has a lower Total Harmonic Distortion (THD) than the PI-controller system, nearly unity power factor, and complies with the IEEE-519 standard. Therefore, the proposed control strategy allows for maximum power extraction from renewable energy resources, regulates the DC-link voltage stably, and enhances the grid-side performance, proving its suitability for modern renewable-energy-integrated electric power systems.*

Keywords *- Artificial Neural Network (ANN), Z-Source Inverter, Wind Energy Conversion System, Permanent Magnet Synchronous Generator (PMSG), DSTATCOM, Power Quality Improvement, Total Harmonic Distortion (THD), Maximum Power Point Tracking (MPPT).*

1. Introduction

A primary reason for the increase in demand for renewable energy is the urgency to lower greenhouse gas emissions, address climate change, and provide sustainable energy for long-term consumption. With wind, solar, and hydropower being an increasing portion of the world's total energy supply, utilities and grid operators face new issues with respect to maintaining stability, reliability, and quality of power. Wind energy has become one of the most adopted forms of renewable energy globally because of its abundance, renewability, and relatively low cost. As utilities continue their transition to using renewable energy as their base load fuel, the way that utilities operate and design their power grids will begin to change [1]. Most modern renewable generators connect to the utility grid via power electronic converters; this has caused many utility networks to contain mostly converter-based systems. Of all the different forms of renewable energy available to consumers, wind energy has gained popularity due to its widespread availability and abundance. Therefore, there has been a substantial increase in the number of large-scale high-power wind farms over the past decade. Solar energy is also a key form of renewable energy; however, it is only able to generate electricity when daylight is available, therefore rendering it useless at night. Variable speed wind turbines can be either DFIG or PMSG. DFIGs are typically less reliable than PMSGs because they employ a slip ring and

brush assembly, which results in mechanical wear and requires maintenance [2-4]. Additionally, DFIGs are capable of operating within a very narrow speed range (±30% around synchronous speed), limiting the amount of energy that can be extracted from a given wind condition.

Furthermore, DFIGs are generally equipped with a gearbox to allow the turbine and generator to run at different speeds; this adds additional mechanical complexity and increases maintenance costs. Because the stator of a DFIG is connected directly to the grid, the DFIG is susceptible to grid faults and voltage disturbances, affecting stability. PMSG has a number of advantages when compared to DFIG, including: higher performance, reduced maintenance requirements when compared to DFIG, and the ability to operate as a direct drive system [5]. Direct drive operation does not require a gearbox; therefore, it reduces mechanical loss and increases the reliability of the system. A comprehensive overview of commercially available PMSG- and DFIG-based wind turbines can be found in [6].

Wind turbines use Doubly Fed Induction Generators (DFIGs), which draw reactive power from the grid due to the direct connection to the stator; therefore, an auxiliary reactive power compensation using a capacitor or STATCOM is needed to maintain the grid stability and improve the overall performance of the system. As a result of the need for reactive power compensation, DFIG-based wind turbines are more dependent upon the grid for voltage support, especially when there are variations in wind speed or the occurrence of grid faults. Permanent Magnet Synchronous Generators (PMSGs) are self-excited due to the presence of the permanent magnet and therefore do not inherently consume reactive power, making them more suitable to be integrated into the grid compared to DFIG-based wind turbines. The main objective of Wind Energy Conversion Systems (WECSs) is to obtain the maximum amount of power available in the wind and provide high-quality electric power to the utility grid.

To achieve this goal, advanced power electronic interfaces are required, and among the most widely used topologies for WECSs is the AC–DC–AC converter [8], which permits the variable-speed operation of wind turbines to optimize the power extraction from the wind at different wind speeds while providing stable grid frequency and voltage [9]. Widespread application of the AC–DC–AC converter has been responsible for significant improvement of both system efficiency and grid reliability [10]. Power electronic converters are playing a critical role in the realization of efficient energy extraction and reliable grid integration in modern wind energy conversion systems. A common configuration of the power electronic converters used in the wind energy conversion systems is the Voltage Source Converter (VSC). Although the traditional VSC offers some advantages, it also has its own disadvantages. When the VSC performs the function of a buck-type inverter during the process of DC-to-AC conversion, the DC-link voltage should be greater than the grid voltage; in addition, when two switches in a phase-leg conduct simultaneously, they can cause short-circuit faults, resulting in damage to the inverter. To prevent the occurrence of shoot-through faults, a dead time is inserted between the switching transitions; however, the insertion of dead Time will cause the degradation of power quality and increase the current distortion [11].

In order to overcome the “buck-type” limitation of WECSs, a two-stage conversion system is generally used. As an example, the three-phase diode bridge can act as a rectifier for the Machine-Side Converter (MSC). However, at low wind turbine speeds, this type of unregulated rectifier likely fails to provide enough DC voltage for the Grid-Side Converter (GSC) to operate effectively and maximize the amount of power that can be extracted from the wind turbine. In order to resolve this issue, a DC–DC boost converter can be used to elevate the output voltage to the desired level, allowing for the highest possible power extraction from the wind turbine. Although this method is relatively inexpensive and easy to implement, it introduces several problems, such as large amounts of harmonic currents flowing through the generator winding, excessive heating, and torque oscillation, illustrating the need for more sophisticated power electronics for use in today’s wind energy systems.

The PMSG can be connected to the grid via two two-level Voltage Source Converters (VSCs) configured in a Back-To-Back (B2B) configuration with Pulse-Width Modulation (PWM) control. Typically, a voltage transformer is included between the Grid-Side Converter (GSC) and the grid in order to match the voltage requirements between the GSC and the grid. This configuration is typically simple, robust, and reliable; however, it has several disadvantages, such as larger switching losses, decreased efficiency at high power levels, and increased Total Harmonic Distortion (THD) [2]. To alleviate these deficiencies associated with traditional two-stage DC–DC boost converters and VSCs, the Z-Source Converter (ZSC) topology was developed as a viable alternative for WECSs [12]. The ZSC has a unique impedance network comprised of inductors and capacitors, which enables the ZSC to perform either a voltage buck or a voltage boost within a single-stage configuration. This distinct feature permits effective power transfer between the energy source and the load without the requirement for an additional DC–DC converter.

Due to its single-stage operation, the ZSC provides numerous benefits, including enhanced reliability, fewer components, smaller size, and lower overall system cost [13]. The ability of ZSI to regulate the output voltage independently of the input voltage makes it a suitable option for the renewable energy technologies that we mentioned above. Also, they can sustain “shoot through” states in each leg of the inverter without causing damage to the switches, therefore

making the overall system more reliable and requiring less dead Time to be utilized. The use of a shoot-through duty cycle allows the ZSC to increase the DC link voltage and to eliminate dead Time, resulting in lower Total Harmonic Distortion (THD) and higher quality of power. In recent years, ZSIs have been increasingly used in variable frequency drives and power conversion systems operating on a fixed DC voltage level. Renewable energy applications have also become an increasingly important area for ZSIs. Two independent control parameters are typically used to control these inverters, namely, the shoot-through Duty Ratio (D_0) and the Modulation Index (m). SBPWM (Simple Boost Pulse-Width Modulation) is the most commonly used method to control the inverter bridge.

The PWM technique will convert null states into shoot-through states, leaving the active-interval states unchanged, thereby eliminating the possibility of short-circuiting or damage to devices and substantially improving the reliability of the inverter. The P&O algorithm has been implemented to optimize energy extraction by implementing MPPT for the wind turbine.A proposed Artificial Neural Network (ANN) controller for determining the shoot-through duty ratio and regulating the DC link voltage is also utilized to provide the d-q axis synchronous current reference. The proposed advanced control method is intended to allow the inverter to operate with a unity power factor under variable wind speed conditions and to provide the maximum possible power to the grid. The proposed ANN-based methodology was evaluated using MATLAB / Simulink simulations, which demonstrated an improvement in reliability, power quality, and efficiency of energy transfer in WECS applications. The recent increased usage of power electronic converters and nonlinear loads in the modern distribution systems has resulted in many new challenges for maintaining Power Quality (PQ) within the acceptable limits established by the grid standards [14-15].

The power electronic converters are commonly responsible for introducing current-related PQ problems, specifically harmonic distortion and load imbalance [16-17], that can lead to higher losses on transmission lines and transformers, distorted voltages, lower system efficiency, and other negative impacts. As well, the introduction of renewable energy sources into the electric grid has introduced voltage-related PQ problems, such as voltage variations, voltage sags, voltage swells, imbalance, and flicker. If voltage variations exceed allowable limits, they can cause sensitive equipment to malfunction or not function at all, resulting in unreliable operation [18-19]. Therefore, various compensation methods have been developed to help solve PQ problems, including Fixed Capacitors (FC), Static VAR Compensators (SVC), DSTATCOM, Dynamic Voltage Restorers (DVR), and Unified Power Quality Conditioners (UPQC). Due to their fast response time, flexibility in control, and ability to correct both voltage and current-related PQ problems, DSTATCOMs are considered one of the most effective compensation solutions [20-22]. There are two primary operating control modes of the DSTATCOM: they are Current Control Mode (CCM) and Voltage Control Mode (VCM). The DSTATCOM operates in CCM primarily to address current-related PQ issues at the Point of Common Coupling (PCC). The increased number of nonlinear loads present in today's electrical distribution systems (i.e., rectifiers, variable speed drives, and power electronic converters) introduces significant amounts of harmonic current into the system [23, 24]. These harmonics significantly distort both the supply current and voltage waveforms, resulting in additional system losses and lower overall efficiencies of the grid-connected equipment. Using a DSTATCOM to operate in CCM, it produces compensating currents that counteract the reactive, harmonic, and unbalanced components of the load current.

As a result, the source currents become balanced, sinusoidal, and in-phase with the corresponding supply voltages to maintain a Unity Power Factor (UPF) at the PCC [25, 26]. Developing a conventional PI controller for a DG system does require an accurate mathematical model to represent the system dynamics and varying load characteristics. However, traditional PI controllers do not perform well under the rapid changes associated with the grid and nonlinear load behavior. Researchers have been studying and developing "intelligent" control methods for DSTATCOM systems to enhance their dynamic responses, adaptability, and overall Power Quality (PQ). ANN has developed as a promising method for designing controllers for power quality improvement devices [27]. The proposed work designs a DSTATCOM with an ANN-based controller to enhance the performance of a DG system that includes wind energy resources [28]. The ANN-based controller effectively addresses current-related PQ issues, ensuring compliance with IEEE-519 standards [29]. Results from MATLAB simulations demonstrate that the ANN-based controller offers superior PQ improvements and dynamic performance.

This work mostly contributes to the following areas:

- Single-stage buck-boost capability with no extra DC/DC converters has been provided through the use of a ZSI in a PMSG-based single-stage grid-connected system.
- Decoupled regulation of the shoot-through duty cycle and modulation index of the ZSI is made possible by an adaptive ANN controller, which provides a unity power factor, constant dc link voltage, and maximizes wind power production regardless of the wind speed.
- Current related power quality problems at the PCC are mitigated with the inclusion of a shunt-connected DSTATCOM controlled by an ANN controller that can compensate for harmonic currents, reactive power, and load imbalance due to nonlinear and variable loads.
- The performance of the proposed ANN-controlled system is much better than the performance of conventional PI-based controllers when subjected to wind speed fluctuations and other types of grid disturbances (e.g.,

voltage sags), because it produces faster settling times, less transient oscillation, and better damping than conventional PI-based controllers.

2. Proposed System Configuration

A variable-speed WECS is used by the new system, which utilizes a PMSG that is directly driven by the WECS, as shown in Figure 1. This removes the need for a gearbox, thereby greatly reducing mechanical loss. The PMSG is connected to the grid via a Back-To-Back (B2B) Voltage Source Converter (VSC), which includes a ZSC. The B2B VSC enables both voltage buck and boost operations in a single stage. The Machine-Side Converter (MSC) utilizes a Maximum Power Point Tracking P&O based algorithm to extract the maximum amount of power from the wind. The Grid-Side Converter (GSC) controls the DC link voltage and maintains stable voltage and frequency at the PCC. The MSC utilizes PWM (pulse width modulated) current control on the d-q axes to maintain a unity power factor condition. The ANN-controlled ZSC adjusts the shoot-through duty cycle of the ZSC to improve DC link voltage stability and the dynamic Response of the system. In addition to the above, an ANN-controlled DSTATCOM provides compensation for the reactive power, harmonics, and load unbalances; therefore, it provides balanced and sinusoidal current flow into the grid as per the IEEE-519 standard.

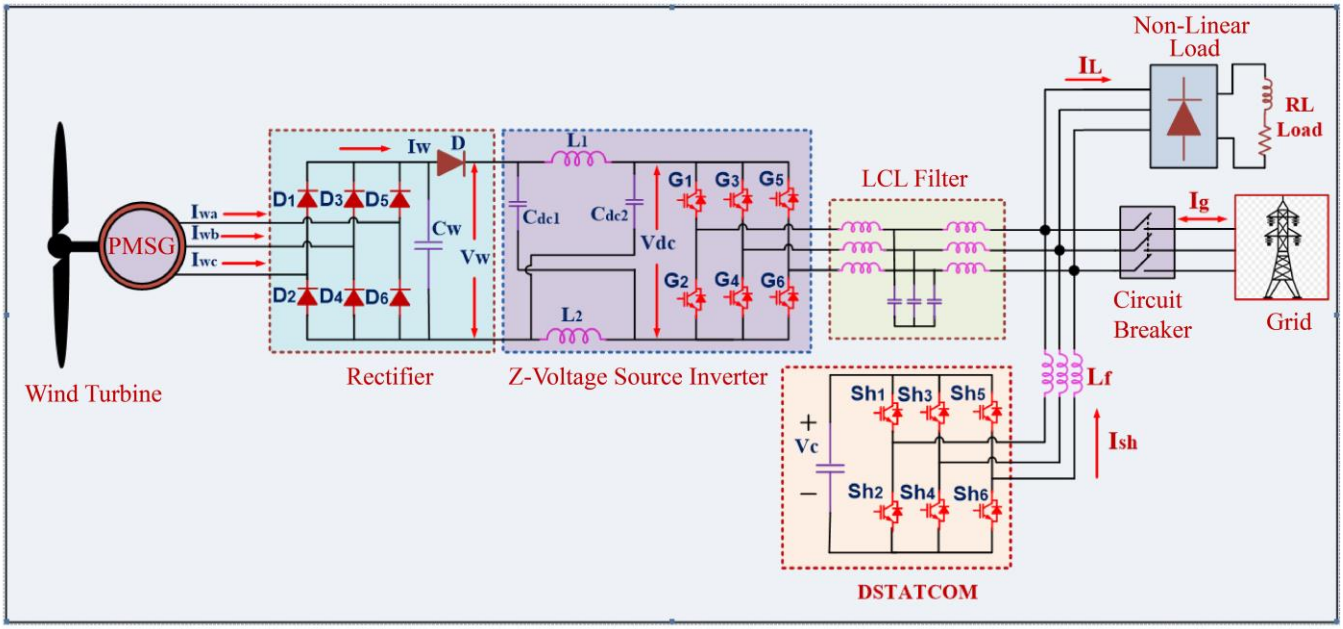

Fig. 1 Proposed grid-connected wind system with ZS network and DSTATCOM

3. Modelling of Wind Power Generation System

3.1. Wind Turbine Aerodynamic Modeling

Wind Energy Conversion Systems (WECS) convert wind-generated kinetic energy into mechanical energy by rotating a turbine rotor. The aerodynamics of WECS play a key role in defining both the efficiency with which the system converts wind to useful mechanical work and the overall dynamic Response of the system, as shown in Figure 2. Aerodynamic models are important to develop control schemes, like MPPT, pitch control, and torque regulation, that optimize WECS performance under various wind conditions. However, wind energy conversions are constrained by Betz's law, indicating that theoretically the most efficient a wind energy conversion can be is 59.3%, and that this efficiency is affected by many aerodynamic factors, including but not limited to rotor design, the tip-speed ratio, and the pitch angle of the blades, and these factors affect the power coefficient. C_P (λ, β), which is defined as the fraction of the wind power that is converted into useful mechanical power.

3.1.1. Aerodynamic Energy Conversion Principle

As the wind moves over the rotor blades, it creates lift and drag forces because of the shape of the blades. The lift force mainly creates torque, while the drag force works against rotation and leads to losses. The total power in the wind that flows through the area swept by the rotor is expressed as

$$P_{wind} = \frac{1}{2}\rho A V_{wind}^3 \quad (1)$$

Where ρ is the air density (kg/m³), A=πR^2 is the swept area of the rotor (m²), R is the rotor radius (m), and V_{wind} is the wind velocity (m/s). The actual mechanical power extracted by the wind turbine is a fraction of the total wind power and is given by:

$$P_m = \frac{1}{2}\rho A C_p(\lambda,\beta) V_{wind}^3 \quad (2)$$

Where $C_p(\lambda,\beta)$ represents the power coefficient as a function of the tip-speed ratio λ and the blade pitch angle β.

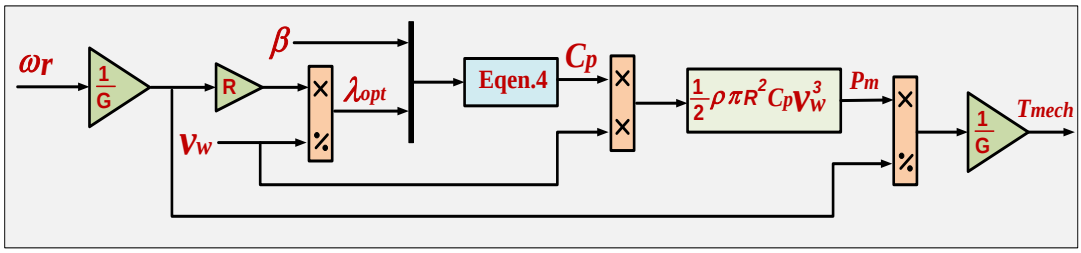

Fig. 2 Wind turbine model

3.1.2. Tip-Speed Ratio (TSR)

The Tip-Speed Ratio is an important aerodynamic measurement that shows how fast the blade tip is moving compared to the actual wind speed. It is defined as

$$\lambda = \frac{\omega_r R}{V_{wind}} \tag{3}$$

Where ω_r is the rotational speed of the rotor (in rad/sec). Every wind turbine has an optimal tip speed ratio (λ_{opt}) for that wind turbine, at which the maximum Power Coefficient (C_p) will be obtained. Operating the turbine at this optimal λ_{opt} allows the turbine to operate with the highest possible aerodynamic efficiency, and also allows the maximum amount of energy to be extracted. Any deviation from λ_{opt} will reduce Cp and therefore result in less power being produced by the turbine due to reduced aerodynamic lift and greater drag.

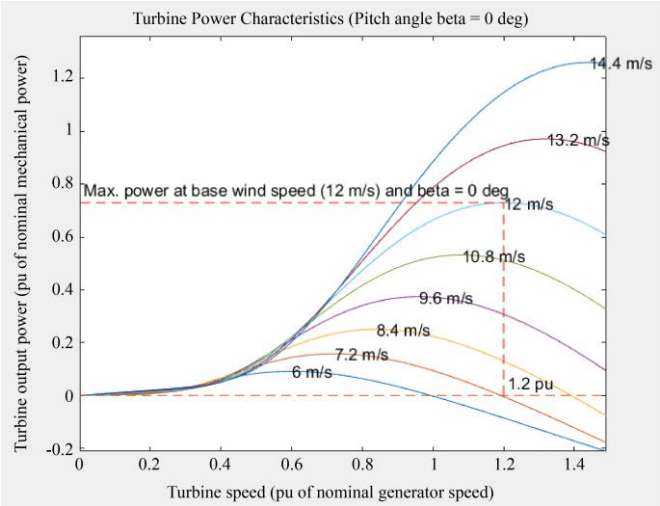

Fig. 3 Turbine power characteristics at different wind speeds with pitch angle β=0∘

3.1.3. Power Coefficient $C_p(\lambda, \beta)$ Characteristics

The aerodynamic efficiency of a wind turbine can be defined by the power coefficient. $C_p(\lambda, \beta)$. This power coefficient is dependent upon both the tip speed ratio (λ) and the blade pitch angle (β), as shown in Figure 4. As a result, Cp is typically found using empirical or semi-empirical relations based upon aerodynamic data. A typical expression for the power coefficient is C_p.

$$c_p(\lambda, \beta) = \left(0.45 - 0.167(\beta - 2)\right) \sin\left(\frac{\pi(\lambda+0.1)}{14.34-0.3(\beta-2)}\right) - 0.00184(\lambda - 3)(\beta - 2) \tag{4}$$

It is often expressed in this analytical form throughout literature due to its accuracy in modeling the nonlinear aerodynamic characteristics of a wind turbine with limited use of lookup tables. The first term defines the primary sinusoidal relationship between C_p Moreover, λ, while the second two terms define the pitch-related corrections of −0.167 (β−2) and −0.00184 (λ−3) (β−2) that modify the amplitude and phase shift of the curve. These correction terms illustrate the influence of the pitch angle upon the aerodynamic performance of the rotor through modification of the effective lift-to-drag ratio and angle-of-attack at which the blades operate [30, 31].

At a fixed pitch angle of β=2∘, the highest C_p is approximately 0.44 when the tip speed ratio λ=8. At this point, there is the best possible operating condition for extracting the maximum amount of energy from the wind under typical conditions.

With increasing pitch angles, the maximum C_p is decreased, which shows how to limit the amount of power that can be extracted by limiting the aerodynamics as the wind speed increases.

3.1.4. Mechanical Power and Torque

Equation (2) yields the mechanical power produced by the turbine rotor, which is transformed into shaft torque via the relationship.

$$T_m = \frac{P_m}{\omega_r} \tag{5}$$

Substituting the value of Pm from Equation (2), the torque can be expressed as:

$$T_m = \frac{1}{2}\rho A \frac{C_p(\lambda,\beta)V_{wind}^3}{\omega_r} \tag{6}$$

This Equation shows that the aerodynamic torque depends on the tip-speed ratio and the square of the wind velocity, highlighting the complex relationship between mechanical output and wind conditions.

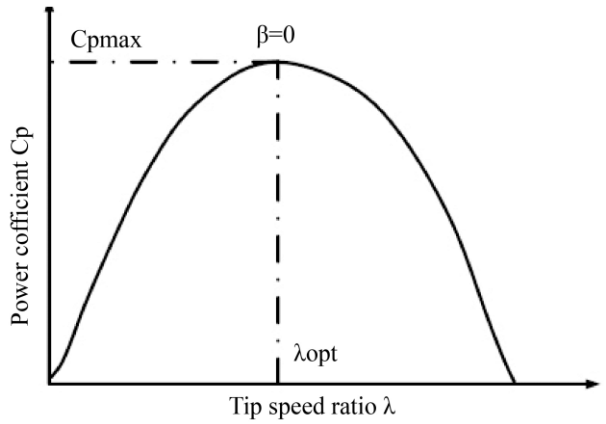

Fig. 4 Power coefficient vs tip speed ratio plot

3.2. Permanent Magnet Synchronous Generator (PMSG) Modeling

PMSGs are currently the most often used generator type in many contemporary WECS because of their high efficiency, compact size, and lack of need for external stimulation. They are perfect for both direct drive and variable speed wind turbines because they eliminate the requirement for field windings and the losses that come with them. The creation of the PMSG's mathematical model and the analysis of its steady state and dynamic functioning are made much easier by the use of a synchronously rotating dq reference frame.

3.2.1. Electrical Equations in the dq Reference Frame

In the rotor reference frame, the stator voltage equations of a PMSG can be expressed as

$$v_d = R_s i_d + \frac{d\psi_d}{dt} - \omega_e \psi_q \quad (7)$$

$$v_q = R_s i_q + \frac{d\psi_q}{dt} - \omega_e \psi_d \quad (8)$$

Where Rs is the stator resistance (Ω), v_d and v_q are the direct-axis and quadrature-axis stator voltages (V), i_d and i_q are the corresponding stator currents (A), ψ_d and ψ_q are the flux linkages (Wb), and ω_e is the electrical angular frequency (rad/s).

The flux linkages in the dq axes are given by

$$\psi_d = L_d i_d + \psi_f \quad (9)$$

$$\psi_q = L_q i_q \quad (10)$$

Where L_d and L_q represent the stator inductances in the direct and quadrature axes (H), and ψ_f is the flux linkage produced by the permanent magnets (Wb). Substituting Equations (9) and (10) into Equations (7) and (8) gives the dynamic voltage model of the PMSG as

$$v_d = R_s i_d + L_d \frac{di_d}{dt} - \omega_e L_q i_q \quad (11)$$

$$v_d = R_s i_q + L_q \frac{di_q}{dt} + \omega_e \left(L_d i_d + \psi_f\right) \quad (12)$$

These equations describe the instantaneous voltage behavior of the PMSG under dynamic operating conditions.

3.2.2. Electromagnetic Torque Equation

The electromagnetic torque developed by the PMSG is given by the following expression:

$$T_e = \frac{3}{2} P\left(\psi_d i_q - \psi_q i_d\right) \quad (13)$$

Substituting Equations (9) and (10) into Equations (11) and (12), the torque equation can be rewritten as

$$T_e = \frac{3}{2} P\left[\psi_f i_q + \left(L_d - L_q\right) i_d i_q\right] \quad (14)$$

In addition to the number of pole pairs as P. Equation (14) shows that the first part of the Equation is the electromagnetic torque generated by the interaction between the stator current and the magnetic field generated by the permanent magnets, and the second part of the Equation is the reluctance torque generated by the saliency of the rotor. When the generator is a non-salient (surface-mounted) PMSG, with $L_d = L_q$Then the torque equation is simplified to (see below).

$$T_e = \frac{3}{2} p \psi_f i_q \quad (15)$$

This shows that the torque is directly proportional to the quadrature-axis current component. i_q, which is the control variable in vector control schemes.

3.2.3. Mechanical Dynamics

The rotational dynamics of the turbine-generator system can be described by Newton's second law as:

$$J \frac{d\omega_m}{dt} = T_m - T_e - B\omega_m \quad (16)$$

Where T_m is the mechanical torque generated by the turbine (N•m), T_e is the electromagnetic torque (N•m), B is the viscous friction coefficient (N•m•s), J is the total inertia of the turbine and generator shaft (kg•m²), and ω_m is the rotor's mechanical angular speed (rad/s). The electrical angular speed and mechanical speed are connected by

$$\omega_e = P\omega_m \quad (17)$$

Equations (16) and (17) describe the dynamic interaction between the aerodynamic torque from the wind turbine and the electromagnetic torque produced by the PMSG.

3.3. AC–DC Diode Rectifier Operation

A Permanent Magnet Synchronous (PMSG) uses wind and rotor speed to produce an alternating voltage with varying frequency and amplitude in a wind energy conversion system. The AC to DC step then changes the AC into a DC that is transmitted or used to send power to the grid. This application's most popular configuration is the three-phase diode bridge rectifier because of its simplicity, efficiency, and variable speed operation. Six diodes arranged in a "bridge" pattern constitute the three-phase diode bridge rectifier as shown in Figure 5.

Each diode conducts for 1/3 of the electrical cycle, which is approximately 120 degrees, depending upon the instantaneous s line-to-line voltage being produced by the generator. At any given time, two diodes, one from the positive leg and one from the negative leg, are conducting simultaneously to allow current to flow from the higher potential to the lower potential. As a result of these conducting cycles, a six-pulse DC waveform is produced at the output of the converter. Although the output voltage is unidirectional, it contains a small ripple, which can be filtered by a DC link capacitor.

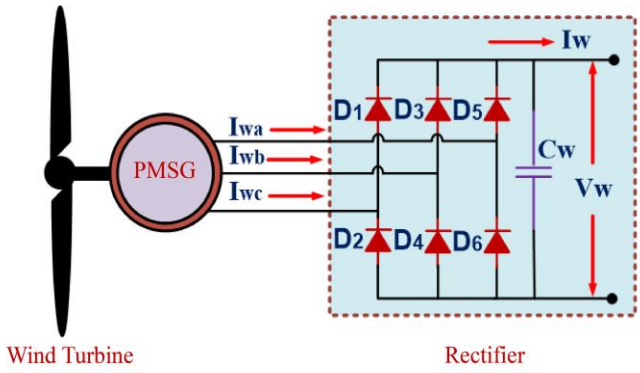

Fig. 5 Designing of AC to DC power conversion

For a balanced three-phase AC supply with an RMS line-to-line voltage denoted by V_{LL}, the average value of the DC output voltage is expressed as

$$V_{DC} = \frac{3\sqrt{2}}{\pi} V_{LL} \tag{18}$$

The output of the three-phase diode-bridge rectifier produces an AC output with a pulsating DC voltage and current, denoted as V_w and I_w respectively. The rectifier's instantaneous output voltage is dependent upon the speed of the generator, and therefore its induced electromotive force; however, since this voltage also has a ripple content due to the commutation of the diodes, a capacitor is used. C_w is connected across the rectifier output to eliminate the ripples from the output voltage and produce a continuous DC voltage to feed the subsequent converter stage.

The DC voltage across the capacitor, denoted as V_w, can be expressed by the following relation

$$I_w = C_w \frac{dV_w}{dt} + I_{load} \tag{19}$$

Where I_w is the current provided by the rectifier, C_w is the DC filtering capacitance, and I_{load} Is the current fed into the DC load connected to the rectifier or the input of the Z-voltage source converter. The capacitor current is given by $I_c = C_w \frac{dV_w}{dt}$, that describes how the capacitor charges/discharges based on the balance between the instantaneous power delivered by the rectifier and the load. During steady state, the capacitor voltage V_w is approximately constant since the average current flowing through the capacitor during each switching cycle is zero. The ripple contained in the DC voltage is determined by the value of the capacitance and the load current, and can be approximated as

$$\Delta V_w = \frac{I_{load}}{f_r C_w} \tag{20}$$

Where f_r is the ripple frequency, typically six times the generator frequency in a six-pulse rectifier. A larger capacitor value reduces the voltage ripple and maintains a nearly constant DC-link voltage.

4. Designing of Z-Voltage Source Converter

The Z-source converter is a high-performance Power Conditioning System (PCS) designed for power conditioning applications that integrate into one stage the functionality of voltage-boosting and voltage-inversion. The Z-source converter is placed between the rectifier output and the inverter bridge to circumvent the limitation of conventional VSCs that do not have the ability to withstand the shoot-through state. The impedance network of the ZSC forms a unique path of energy transfer that allows controlled shoot-through states, while also providing the capability of voltage boosting and improving the overall reliability of the system.

4.1. Z-Source Inverter Design and Modeling

The first stage of the proposed system is the smoothing of the rectified DC voltage from the wind source. V_w and the associated current I_w provided by the Diode Rectifier. To lower the voltage ripple connected to the Diode Rectifier output, a DC Filter Capacitor is used. C_w is employed. The Z-source Network, which consists of two inductors L_1 and L_2 and two capacitors C_{dc1} and C_{dc2} arranged in an "X" form between the DC Source and the Inverter Bridge, receives the filtered DC power after that. The inductors are located in the top and bottom arms of the Network, while the capacitors are located diagonally to form a symmetric Energy storage circuit that maintains a balanced DC Link Voltage, as shown in Figure 6. Typically, under steady-state symmetrical operations, the Parameters are assumed to be L_1=L_2=L and C_{dc1}=C_{dc2}=C_{dc}. Each capacitor's voltage is denoted by V_c,

while the DC link voltage across the inverter bridge is denoted by $V_{dc-link}$. The shoot-through mode and the non-shoot-through mode are the two distinct operating modes of the ZSI.

4.1.1. Shoot-Through (ST) Mode Operation

Both of an inverter leg's switches are conducting simultaneously during the shoot-through state, which short-circuits the inverter bridge as shown in Figure 7. The Z-source Impedance Network's diode is reverse-biased. As a result of the current being drawn, the inductors L_1 and L_2 will store energy, and the capacitors C_{dc1} and C_{dc2} will discharge through the inductors. The equivalent circuit of this state may be defined using the following voltage and current relationships:

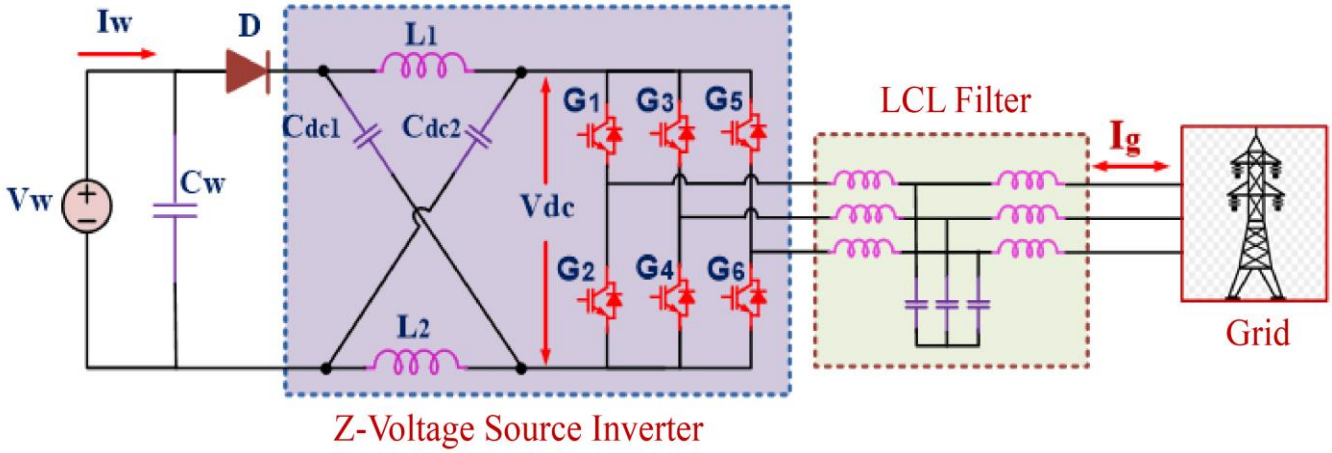

Fig. 6 Designing of grid-connected Z-voltage source inverter

Table 1. Simulation parameters of ZSI

Parameters	Values
Grid Voltage	230 V
Grid frequency f_g	50 Hz
Inductor of ZSI L_1, L_2	1000 µH
Capacitor of ZSI C_{dc1}, C_{dc2}	1000 µF
Switching frequency f_s	10 KHz
Interface Inductor (L_f)	500 µH
Filter Capacitor (C_f)	100 µF

$$v_{L1} = V_w + V_{C2} \quad (21)$$

$$v_{L2} = V_{C1} \quad (22)$$

$$V_{DC-link} = 0 \quad (23)$$

$$i_{C1} = -i_{L2} \quad (24)$$

$$i_{C2} = -i_{L1} \quad (25)$$

Here, V_w denotes the DC voltage obtained from the rectified output of the wind generator. In this mode, the energy transfer occurs from the capacitors to the inductors, allowing the inductors to store magnetic energy. The DC-link voltage remains zero since the inverter bridge is short-circuited.

4.1.2. Non-Shoot-Through (Non-ST) Mode Operation

The inverter functions as a typical VSI and provides power to the grid or AC load during the non-shoot-through interval. As the inductors release their stored energy, the diode in the Z-network becomes forward-biased, allowing the input source to replenish the capacitors. The voltage and current equations governing this mode are given as:

$$v_{L1} = V_w - V_{C1} \quad (26)$$

$$v_{L2} = -V_{C2} \quad (27)$$

$$V_{DC-link} = V_{C1} + V_{C2} \quad (28)$$

$$i_{C1} = i_{L1} - i_{DC} \quad (29)$$

$$i_{C2} = i_{L2} - i_{DC} \quad (30)$$

The inverter operates conventionally, converting the boosted DC-link voltage into an AC output. The inductors discharge, supplying both the load and recharging the capacitors, thereby maintaining a balanced and stable DC-link voltage.

4.1.3. Voltage Boost Relationship

By using the volt-second balance principle across the inductors L_1 and L_2 For a single switching cycle T, which includes both shoot-through and non-shoot-through durations, the Z-source network's voltage boost capability is determined. The expression for the inductor voltage balance is:

$$(V_w + V_{C2})D_s + (V_w - V_{C1})(1 - D_s) = 0 \quad (31)$$

Where Ds is the shoot-through duty ratio, solving for the capacitor voltages gives:

$$\frac{V_{C1}}{V_w} = \frac{1-D_s}{1-2D_s} \quad (32)$$

$$\frac{V_{C2}}{V_w} = \frac{D_s}{1-2D_s} \quad (33)$$

The total boosted DC-link voltage can thus be obtained as:

$$V_{DC-link} = V_{C1} + V_{C2} = \frac{V_w}{1-2D_s} \quad (34)$$

The boost factor (B) of the Z-source inverter is defined as:

$$B = \frac{1}{1-2D_s} \quad (35)$$

The DC-link voltage can be expressed as:

$$V_{DC-link} = BV_W \quad (36)$$

The boost factor B increases with the shoot-through Duty Ratio (D_s); however, to prevent overvoltage stress on passive elements, D_s is typically limited to ensure B remains within a safe range.

4.1.4. Inverter AC Output Voltage

The inverter uses sinusoidal PWM modulation to transform the increased DC-link voltage into a three-phase AC output.

The following provides the basic component of the inverter output phase voltage:

$$v_{ac} = \frac{MV_{DC-link}}{2} = \frac{MBV_m}{2} \quad (37)$$

Where M is the modulation index (0<M<1). Therefore, the overall voltage gain (G) of the Z-source inverter is expressed as:

$$G = M \times B \quad (38)$$

Thus, the inverter output voltage becomes:

$$v_{ac} = \frac{GV_w}{2} \quad (39)$$

This relationship shows that, unlike a conventional VSI, the ZSI can boost and invert simultaneously within a single stage. The shoot-through state enables a variable DC-link boost, while the modulation index controls the AC output amplitude, ensuring superior voltage control flexibility.

4.1.5. Current Relations and Input Characteristics

The inductor currents in the steady-state condition can be represented as:

$$I_{L1} = I_{L2} = I_{dC}\frac{(1-D_s)}{(1-2D_s)} \quad (40)$$

Moreover, the input current during the non-shoot-through period is:

$$I_{in} = \frac{I_{L1}}{(1-D_s)} = I_{dc}\frac{(1-D_s)}{(1-2D_s)(1-D_s)} = I_{dc}\frac{1}{(1-2D_s)} \quad (41)$$

As Ds increases, the inductor current rises, corresponding to greater stored energy and higher voltage boost across the inverter DC-link.

The inductors L_1 and L_2 They are designed to limit the current ripple to a specified percentage of the average inductor current, typically 20%–30%. The required inductance value is calculated as:

$$L = \frac{V_C D_s}{\Delta I_L f_s} \quad (42)$$

Where f_s is the inverter's switching frequency and ΔI_L is the peak-to-peak inductor current ripples. The capacitors C_{dc1} and C_{dc2} They are designed to ensure that the voltage ripple remains within acceptable limits. The required capacitance value is given by:

$$C_{dc} = \frac{I_{DC-link}D_s}{\Delta V_c f_s} \quad (43)$$

Where $I_{DC-link}$ The current flowing through the DC-link is ΔV_c is the allowable voltage ripple across the capacitors. Larger capacitance values reduce voltage fluctuations and maintain balanced capacitor voltages under dynamic operating conditions.

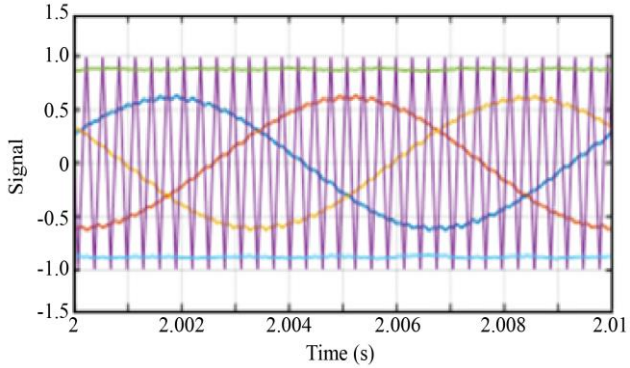

Fig. 7 Description of the SBPWM

The Z-source impedance network serves as both an energy storage and boost interface, allowing the inverter to manage shoot-through conditions safely while delivering a

stable and increased DC-link voltage. The DC filter capacitor C_ω smooths the output from the rectifier, while the Z-source capacitors C_{dc1} and C_{dc2} Maintain the necessary balance of the DC-link voltage. This setup boosts voltage stability, improves dynamic performance, and guarantees reliable operation of the wind energy system connected to the grid.

4.2. Control Design of Z-Voltage Source Converter

The layout of the controls shown in Figure 6 is a control method based on an ANN for a ZSI that is connected to a wind energy system powered by a PMSG. Several steps of the controller work together to make sure that the grid is in sync, that the maximum power point is tracked, that the DC link voltage is regulated, that the dq axis current is controlled, that modulation indexes are generated, and that gate pulses are produced, as shown in Figure 10.

4.2.1. Maximum Power Point Tracking Stage

The Perturb and Observe algorithm first identifies the reference Wind Side Voltage V_w^* corresponding to the maximum power point by observing the change in output power with respect to voltage, as shown in Figure 8, presents a flow chart of the P&O MPPT algorithm [32-33]. The instantaneous power is obtained from the measured wind voltage and current as:

$$P_w = V_w I_w \tag{44}$$

The incremental power change determines the direction of adjustment of the reference voltage.

$$\frac{dP}{dV} > 0 \Rightarrow V_w^* increases \tag{45}$$

$$\frac{dP}{dV} < 0 \Rightarrow V_w^* decreases \tag{46}$$

To improve dynamic Response and reduce steady state oscillations, an Artificial Neural Network is used to refine the reference voltage according to the nonlinear relationship.

$$V_{w,ref} = f_{ANN}(\Delta P, \Delta V) \tag{47}$$

The ANN continuously adapts to varying wind speed and generator operating conditions to provide a smooth and optimal reference for the DC side converter.

4.2.2. Outer DC Link Voltage Control Loop

The DC voltage from the Z source impedance network is maintained at a constant level to ensure stable inverter operation. The voltage error is calculated as:

$$e_{dc}(t) = V_{dc}^* - V_{dc} \tag{48}$$

This error signal is processed by an ANN regulator that produces the reference d-axis current.

$$I_d^* = f_{ANN}(e_{dc}, \dot{e}_{dc}) \tag{49}$$

The ANN replaces the conventional proportional-integral controller and provides faster transient Response and adaptive tuning during nonlinear and dynamic conditions.

4.2.3. Inner Current Control Loop

The synchronous reference frame transformation converts the measured grid voltages and currents from the abc frame into the dq frame using the grid angular position obtained from a phase-locked loop. The transformation equations are

$$V_d = \frac{2}{3}(V_a + V_b \cos 120^0 + V_c \cos 240^0) \tag{50}$$

$$V_q = \frac{2}{3}(V_a + V_b \sin 120^0 + V_c \sin 240^0) \tag{51}$$

$$\begin{bmatrix} I_d \\ I_q \end{bmatrix} = \frac{2}{3}\begin{bmatrix} \cos(\theta) & \cos\left(\theta - \frac{2\pi}{3}\right) & \cos\left(\theta + \frac{2\pi}{3}\right) \\ -\sin(\theta) & -\sin\left(\theta - \frac{2\pi}{3}\right) & -sin\left(\theta + \frac{2\pi}{3}\right) \end{bmatrix}\begin{bmatrix} I_a \\ I_b \\ I_c \end{bmatrix} \tag{52}$$

The dq axis reference currents are compared with the measured currents to obtain current errors.

$$e_d = I_d^* - I_d \tag{53}$$

$$e_q = I_q^* - I_q \tag{54}$$

and their derivatives as

$$\dot{e}_d = \frac{d}{dt}(e_d) \tag{55}$$

$$\dot{e}_q = \frac{d}{dt}(e_q) \tag{56}$$

These errors are processed by two independent ANN controllers to determine the reference dq-axis voltages. V_d^* and V_q^*. The ANN controller outputs are given by

$$V_d^* = f_{ANN}(e_{d,}\dot{e}_d) + \omega L I_q + V_d \tag{57}$$

$$V_q^* = f_{ANN}(e_{q,}\dot{e}_q) + \omega L I_d + V_q \tag{58}$$

Here, L represents the filter inductance and ω is the grid angular frequency obtained from the PLL. The cross-coupling terms ($\omega L I_q$) and ($\omega L I_d$) ensure proper decoupling between the d and q axes, improving current control accuracy.

The inclusion of grid voltages V_d and V_q The control law helps in achieving better synchronization and stable power injection into the grid.

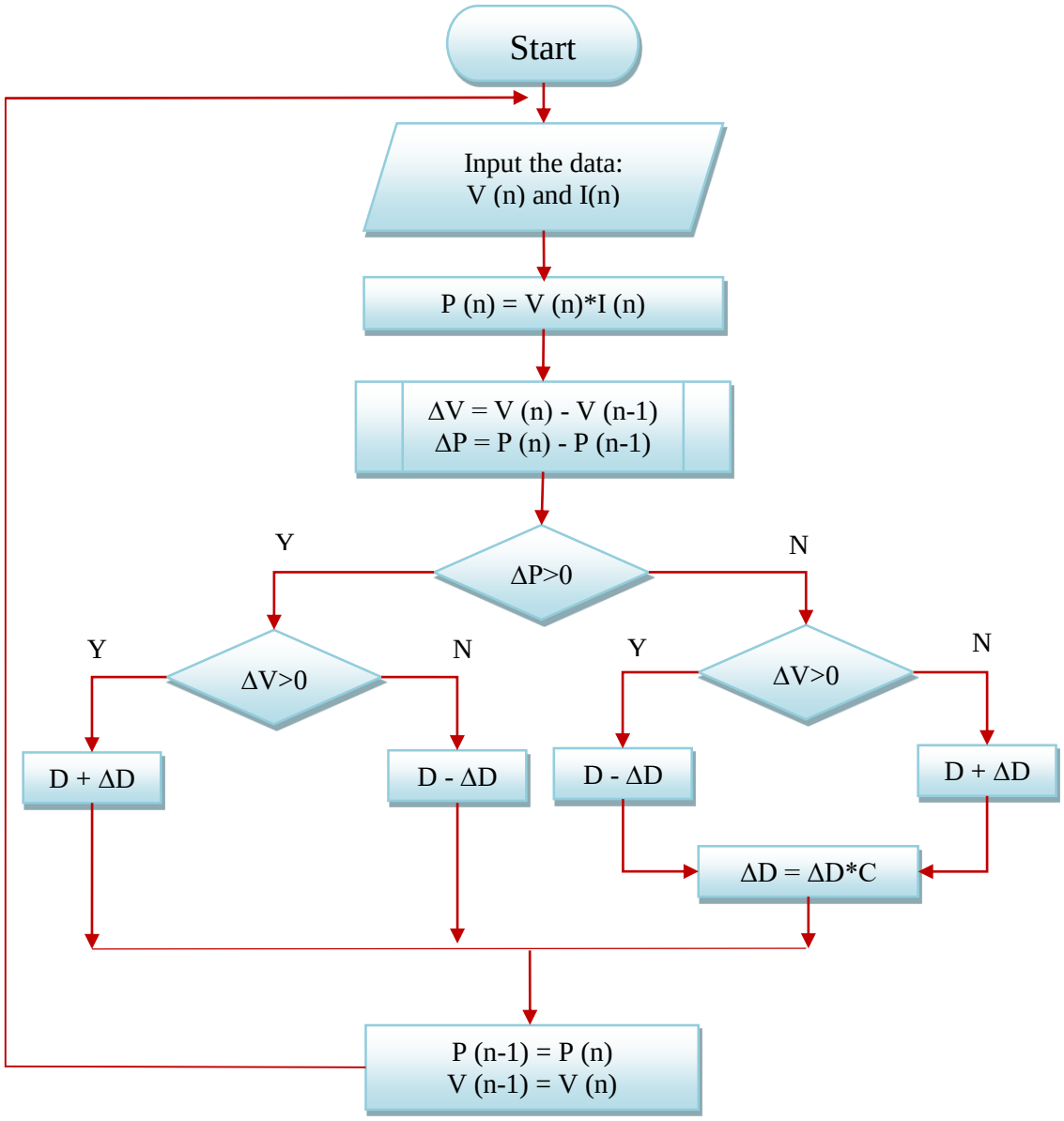

Fig. 8 The MPPT's perturb and observe technique flow chart

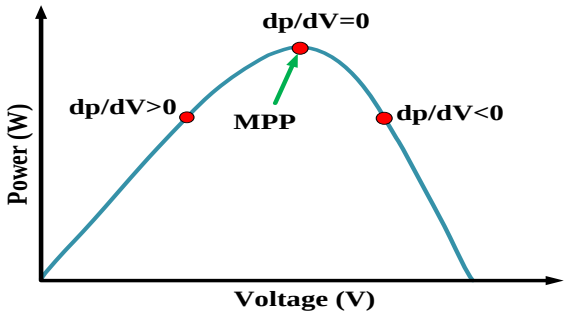

Fig. 9 Plot of wind power vs wind voltage

4.2.4. Generation of Reference Modulation Signals

The reference dq-axis voltages V_d^* and V_q^* are converted into modulation signals m_d^* and m_q^* as

$$m_d^* = \frac{\sqrt{(V_d^*)^2+(V_q^*)^2}}{V_{dc}} \quad (59)$$

$$m_q^* = \tan^{-1}\left(\frac{V_q^*}{V_d^*}\right) + \omega t \quad (60)$$

These quantities define the amplitude and phase required to synchronize the inverter output voltage with the grid voltage. The dq-axis reference modulation signals m_d^* and m_q^* are generated by the control loops that regulate current or voltage based on system requirements. These references are transformed into three-phase sinusoidal modulation signals. M_{abc} through the inverse Park–Clarke transformation, expressed as:

$$\begin{bmatrix} m_a \\ m_b \\ m_c \end{bmatrix} = \begin{bmatrix} \sin(\omega t) \\ \sin(\omega t - 120°) \\ \sin(\omega t + 120°) \end{bmatrix} \cdot \left(m_d^* + j m_q^*\right) \quad (61)$$

The grid's electrical angle is represented by ωt. To create PWM switching pulses for the inverter switches, these sinusoidal signals M_{abc} are compared to a high-frequency carrier (triangular) waveform. The wind-side operating point is continuously modified by the P&O Maximum Power Point Tracking algorithm. It keeps the DC-link voltage. $V_{DC-link}$ at the ideal level to harvest the most power possible from the wind turbine generator by adjusting m_d^* and m_q^*.

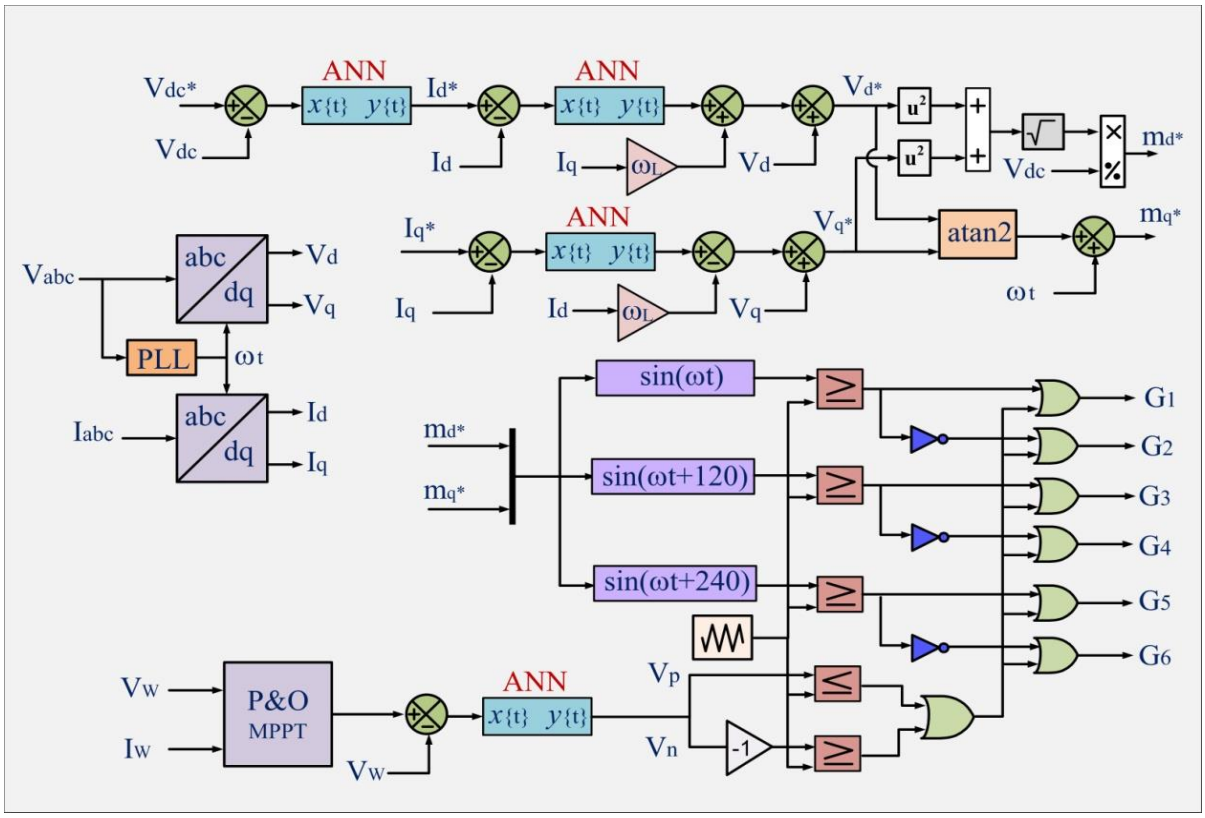

Fig. 10 Control strategy of Z-Voltage source converter

4.2.5. Shoot-Through State Generation

In order to activate the voltage boosting function, the inverter purposefully introduces a Shoot-Through (ST) state. This scenario occurs when one or more inverter legs' two switches are turned on at the same Time. Logical OR operations are used to combine the shoot-through gating pulses and the sinusoidal reference signals to create the shoot-through command, as follows:

$$V_{ST} = \left(V_p \; OR \; V_n\right) OR \; M_{abc} \quad (62)$$

Where:

- V_p: positive shoot-through gating pulse,
- V_n: negative shoot-through gating pulse, and
- M_{abc}: Sinusoidal modulation signals.

This logic ensures that the inverter bridge is short-circuited during shoot-through intervals, while normal PWM operation occurs during non-shoot-through periods. This integration preserves the PWM control while allowing voltage boost within the same switching framework.

5. Designing of DSTATCOM

Modern electrical distribution systems are being affected by nonlinear loads like diode rectifiers, variable frequency drives (adjustable speed drives), and switch-mode power supplies, which generate harmonic currents and reactive power demands, resulting in distorted voltages and reduced efficiency within the electrical distribution system. This results in degraded power quality and increased THD at the PCC. To counteract the adverse effects of the nonlinear loads on the electrical distribution system, a DSTATCOM can be used as an Active Power Filter (APF) and as a shunt-connected device. The DSTATCOM injects dynamic compensating currents into the distribution system to provide sinusoidal source currents and a unity power factor, as shown in Figure 11. An Adaptive ANN controller is proposed in this work to improve the dynamic performance of the DSTATCOM for changing load conditions. The ANN controller produces the optimal reference signal for the compensating current so that the DSTATCOM can accurately cancel both the harmonic and reactive power components of the nonlinear load current.

5.1. Measurement and Clarke Transformation

The first phase is to measure the Three-Phase Line Voltages (V_{Labc}) and Current (I_{Labc}). Next, these measurements can be converted from a three-phase system to an orthogonal reference plane in a stationary state (α – β) by means of the Clarke transform. The α-β conversion transforms the three-phase system into a two-axis system that allows for the instantaneous analysis of power and the implementation of digital control strategies.

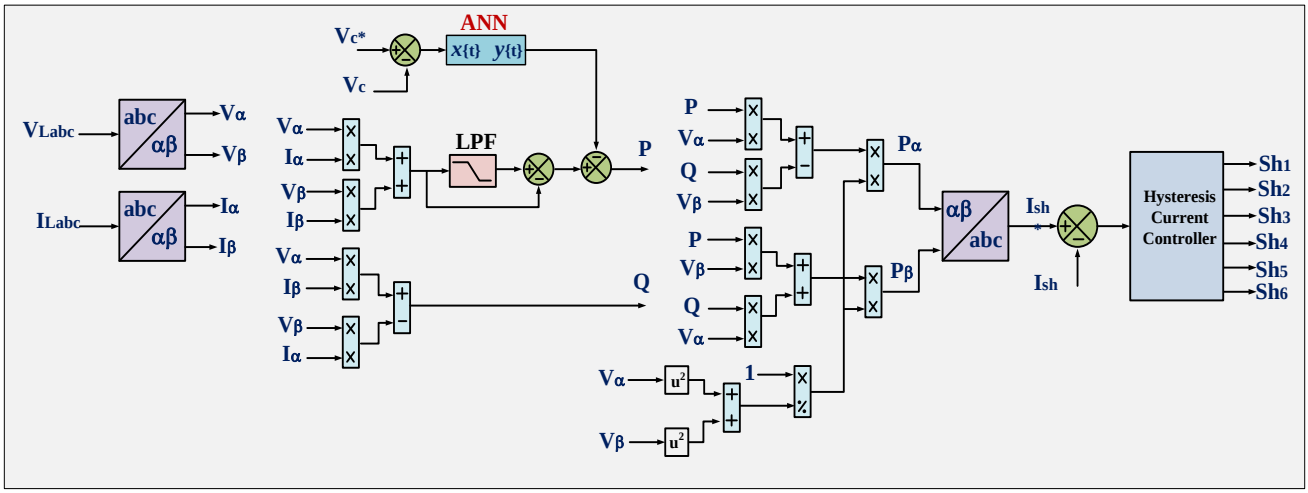

Fig. 11 Control design of active power filter DSTATCOM

$$\begin{bmatrix} V_\alpha \\ V_\beta \end{bmatrix} = \sqrt{\frac{2}{3}} \begin{bmatrix} 1 & -\frac{1}{2} & -\frac{1}{2} \\ 0 & \frac{\sqrt{3}}{2} & -\frac{\sqrt{3}}{2} \end{bmatrix} \begin{bmatrix} V_a \\ V_b \\ V_c \end{bmatrix} \quad (63)$$

Similarly, the Clarke transformation is used to convert the three-phase load currents from the ABC reference frame to the stationary α–β reference frame as

$$\begin{bmatrix} I_\alpha \\ I_\beta \end{bmatrix} = \sqrt{\frac{2}{3}} \begin{bmatrix} 1 & -\frac{1}{2} & -\frac{1}{2} \\ 0 & \frac{\sqrt{3}}{2} & -\frac{\sqrt{3}}{2} \end{bmatrix} \begin{bmatrix} I_a \\ I_b \\ I_c \end{bmatrix} \quad (64)$$

This transformation reduces the three-phase system into a two-dimensional stationary reference frame, thereby simplifying the computation of instantaneous power quantities.

In the α–β reference frame, the instantaneous real and reactive power components are calculated using the instantaneous power theory as

$$P = V_\alpha I_\alpha + V_\beta I_\beta \quad (65)$$

$$Q = V_\beta I_\alpha + V_\alpha I_\beta \quad (66)$$

Where Q stands for the instantaneous reactive power and P for the instantaneous active power. Under nonlinear and unbalanced loading conditions, these power components consist of both DC (fundamental) and AC (oscillating) components. The oscillating components are associated with current harmonics and reactive power demand, which must be compensated by the D-STATCOM.

5.2. Low-Pass Filtering

To isolate the fundamental component of power, the instantaneous active power signal is passed through a first-order Low-Pass Filter (LPF) given by

$$LPF(s) = \frac{\omega_c}{s+\omega_c} \quad (67)$$

Where ω_c is the filter's cutoff angular frequency. The average (fundamental) active power Pf is represented by the filtered output, while the oscillating component is found as

$$\tilde{P} = P - P_f \quad (68)$$

The load's fundamental active power is represented by the DC component, while the harmonic-related power that the D-STATCOM must correct for is represented by the AC component.

5.3. ANN-Based Reference Signal Generation

The proposed ANN controller adaptively generates the reference compensation signal based on real-time system conditions. The ANN receives the DC-link voltage error.

$$e_v = V_c^* - V_c \quad (69)$$

and its derivative

$$\dot{e}_v = \frac{d}{dt}(V_c^* - V_c) \quad (70)$$

As input signals. Based on these inputs, the ANN produces the reference DC-link control signal and compensating power component as

$$P_{dc} = f_{ANN}(e_v, \dot{e}_v) \tag{71}$$

Where $f_{ANN}(\cdot)$ represents the nonlinear mapping learned by the neural Network through adaptive weight tuning. The ANN effectively captures the nonlinear dynamics of the system, enabling fast DC-link voltage regulation, dynamic harmonic suppression, and accurate reactive power compensation.

5.4. Reference Compensation Current Calculation

Based on the instantaneous power theory, the compensating reference currents in the α–β reference frame are calculated as

$$\begin{bmatrix} I^*_{sh\alpha} \\ I^*_{sh\beta} \end{bmatrix} = \frac{1}{V_\alpha^2 + V_\beta^2} \begin{bmatrix} V_\alpha & V_\beta \\ -V_\beta & V_\alpha \end{bmatrix} \begin{bmatrix} \tilde{P} - P_{dc} \\ Q \end{bmatrix} \tag{72}$$

In this case, Q stands for the instantaneous reactive power and $\tilde{P}$ for the oscillatory component of active power. These values establish the reactive power demand of the nonlinear load and the compensatory current needed to remove harmonic currents. To guarantee balanced and sinusoidal source currents, the reference compensating currents in the three-phase abc frame are then acquired for each phase.

5.5. Inverse Clarke Transformation

The inverse Clarke transformation is used to convert the compensatory current references in the α–β frame back into the three-phase ABC frame as

$$\begin{bmatrix} I^*_{sha} \\ I^*_{shb} \\ I^*_{shc} \end{bmatrix} = \begin{bmatrix} 1 & 0 \\ -\frac{1}{2} & \frac{\sqrt{3}}{2} \\ -\frac{1}{2} & -\frac{\sqrt{3}}{2} \end{bmatrix} \begin{bmatrix} I^*_{sh\alpha} \\ I^*_{sh\beta} \end{bmatrix} \tag{73}$$

These reference currents are supplied to the current controller for generating appropriate inverter switching signals.

5.6. Hysteresis Current Controller

The hysteresis current controller ensures that the actual compensating current is maintained. I_{sh} follows the reference current I^*_{sh} within a specified hysteresis band. The instantaneous current error is expressed as:

$$e(t) = I_{sh}(t) - I^*_{sh}(t) \tag{74}$$

The switching logic is as follows:

- If $e(t) > +h$: turn OFF the upper switch of the inverter leg.
- If $e(t) < -h$: turn ON the upper switch of the inverter leg.

Here, h is the hysteresis bandwidth. This controller offers fast dynamic Response and maintains nearly constant switching frequency, ensuring rapid compensation of harmonic currents in real Time.

6. Design of the ANN Controller for Z-Source Inverter and DSTATCOM

An Artificial Neural Network controller was developed for regulating the dc-link voltage of the ZSI, as well as enhancing the ability of the DSTATCOM to compensate for variations in both grid and load conditions. The ANN controller is used in place of a traditional PI controller to provide faster dynamic Response, to improve the ANN's ability to handle nonlinearities adaptively, and to provide better harmonic compensation. The designed ANN has three layers, which are defined as follows: an output layer that gives a single neuron output signal, two hidden layers with five neurons each, and an input layer with three neurons, as shown in Figure 14. The ANN is a multi-layer feed-forward network, and the representation of the network structure can be denoted by [3, 5, 1]. The ANN network was trained utilizing the Levenberg-Marquardt (LM) optimization algorithm because it is able to converge rapidly and to maintain low errors [34, 35].

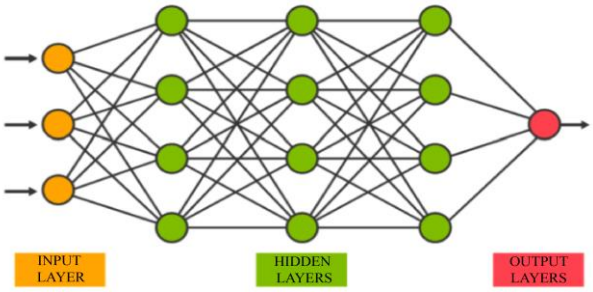

Fig. 12 Design of a backpropagation network to provide a standard reference signal

6.1. Input and Output Selection

The ANN controller receives three normalized input parameters:

$$I = [e(t), \dot{e}(t), e_{int}(t)]^T \tag{75}$$

Where

$$e(t) = V_{dc\_ref} - V_{dC} \tag{76}$$

is the instantaneous voltage error,

$$\dot{e}(t) = \frac{de(t)}{dt} \tag{77}$$

is the derivative of the error, and

$$e_{int}(t) = \int e(t)\,dt \quad (78)$$

is the accumulated error component.

The output of the ANN controller, denoted by u(t), serves as the control signal for:

- Modifying the Z-source inverter's modulation index M and shoot-through duty ratio DST to control DC-link voltage.
- Generating the compensating current reference I^*_{sh} for DSTATCOM to mitigate harmonics and reactive power at the grid interface.

$$u(t) = f_{ANN}(I) \Rightarrow \{D_{ST,}M, I^*_{\text{sh}}\} \quad (79)$$

6.2. Network Structure and Transfer Function

The network output is formulated as:

$$u(t) = f_0\left(\sum_{j=1}^{5} w_{oj} f_h\left(\sum_{i=1}^{3} w_{ji} I_i + b_j\right) + b_o\right) \quad (80)$$

Where $f(x) = \tanh(x)$ is the tangent-sigmoid activation function in the hidden layer, $f_o(x) = x$ is the linear activation function in the output layer, wji and woj represent the connection weights, and b_j, b_o denote the respective bias terms. The input signals are normalized within a defined range using:

$$I_{norm} = \frac{I - I_{min}}{I_{max} - I_{min}} \quad (81)$$

6.3. Training Process

The ANN is trained with the input–output dataset obtained from system dynamics under various operating conditions. The objective is to minimize the Mean Squared Error (MSE) between the predicted output $\hat{T}$ and the target output T:

$$E = \frac{1}{N}\sum_{k=1}^{N}\left(T_k - \hat{T}_k\right)^2 \quad (82)$$

The LM algorithm updates the weight vector iteratively as:

$$w_{k+1} = w_k - [J^T J + \mu I]^{-1} J^T e \quad (83)$$

Where J is the Jacobian matrix of partial derivatives, μ is the damping factor, and e is the instantaneous error vector.

Training is conducted with the following parameters:

- Epochs:1000
- Performance goal:1×10^{-12}
- Training algorithm: LM (trainlm)

Activation function: logsig, tansig, and purelin

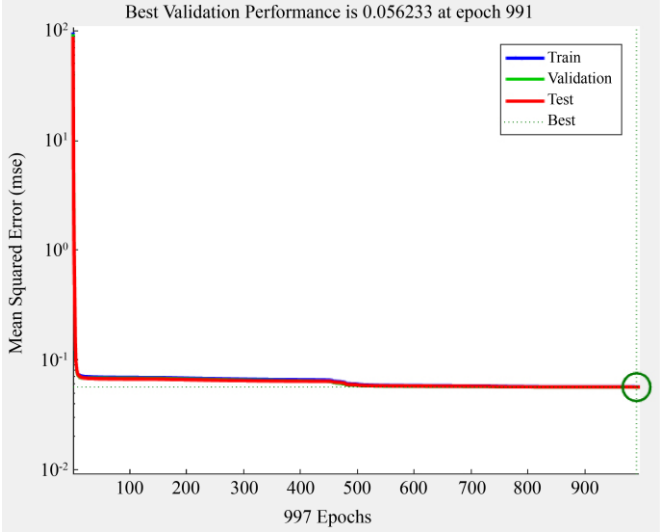

Fig. 13 MSE effect plot of the Artificial Neural Network (ANN) model

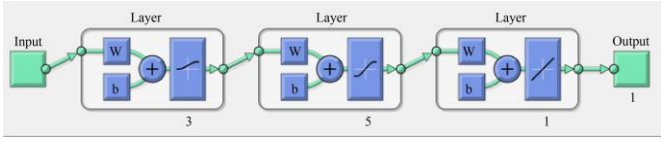

Fig. 14 Structure of Neural Network

6.4. Integration with Control System

Once trained, the ANN replaces the conventional PI regulator in both control loops:

1. Z-Source Inverter Loop: The ANN output uZSI(t) regulates the DC-link voltage by modulating DST and M to maintain a constant inverter input voltage under wind power fluctuations:

$$V^*_{dc} = f_{ANN}(e, \dot{e}, e_{int}) \quad (84)$$

2. DSTATCOM Loop: The ANN output u DSTATCOM(t) generates the reference compensating current I^*_{sh} to minimize harmonic distortion and reactive power at the grid side:

$$I^*_{sh} = f_{ANN}(e, \dot{e}) \quad (85)$$

After training, the optimized weights are fixed for real-time operation. The ANN output dynamically adjusts the modulation index, shoot-through duty cycle (in ZSI), and compensating current (in DSTATCOM) to maintain constant DC-link voltage, unity power factor, and low harmonic distortion.

7. Simulation Results and Discussion

7.1. Dynamic performance of the Proposed ANN-Controlled Wind Energy System

The evaluation of a grid-connected Wind Energy System integrated with ZSI, DSTATCOM, and an Adaptive ANN Controller was performed through MATLAB / Simulink

simulations over a time span of 0.5 seconds. The primary objective of the system was to maintain a DC link voltage of 600 V; however, the DSTATCOM provided reactive power compensation and voltage support to the system, as shown in Figure 15.

A PMSG was used to provide variable power generation based on changes in the wind speeds. Initially, between 0 and 0.2 seconds, the PMSG generated 30 kW of electrical power under a wind speed of 12 m/s, and 10 kW of electrical power were delivered to the load, while 20 kW of electrical power were exported to the grid.

The ANN-controlled inverter successfully maintained a stable supply of electrical power while regulating voltage. Upon a reduction of the wind speed from 12 m/s to 8 m/s at 0.2 seconds, the generation of electrical power decreased (from 30 kW to 22 kW), resulting in a decrease in the amount of electrical power exported to the grid (from 20 kW to 12 kW); however, the load remained at 10 kW.

The ANN controller rapidly adjusted the inverter modulation index to compensate for this disturbance and minimize voltage deviations. During this time frame, the DSTATCOM provided reactive power support to uphold the stability of the voltage. Between 0.35 and 0.5 seconds, the wind speed returned to 12 m/s, increasing the electrical power generation of the PMSG to 30 kW.

The ANN controller successfully restored the system to its steady state and increased the amount of electrical power exported to the grid to 20 kW, while maintaining a consistent DC link voltage.

The simulation results indicate that the ANN controller significantly enhances the dynamic stability of the wind energy system, minimizes transient oscillations, and reduces the settling times when compared to traditional PI controllers. Overall, the integration of the ANN-controlled Z Source Inverter and DSTATCOM has resulted in the enhancement of the overall voltage regulation, balance of power delivery, and improved overall stability of the wind energy system under changing wind conditions.

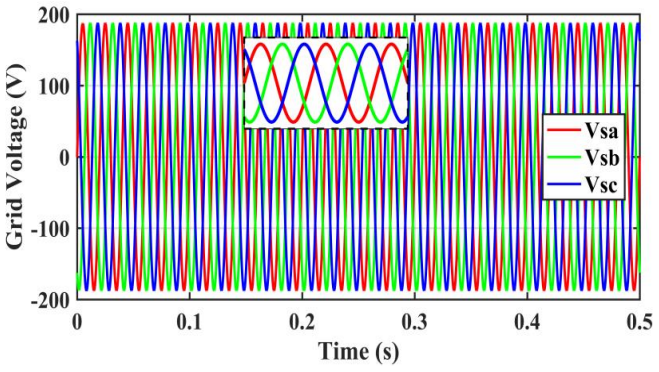

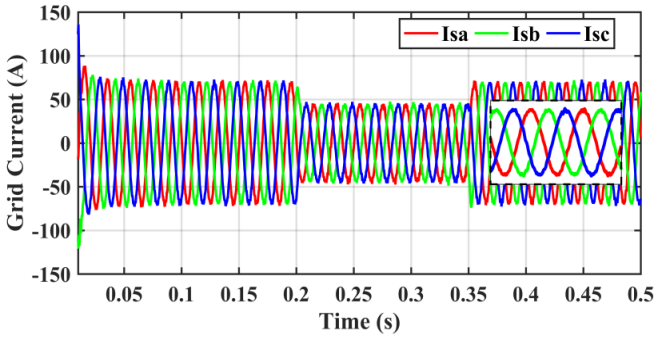

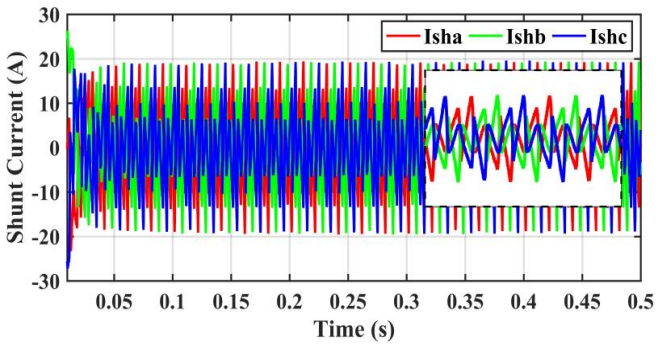

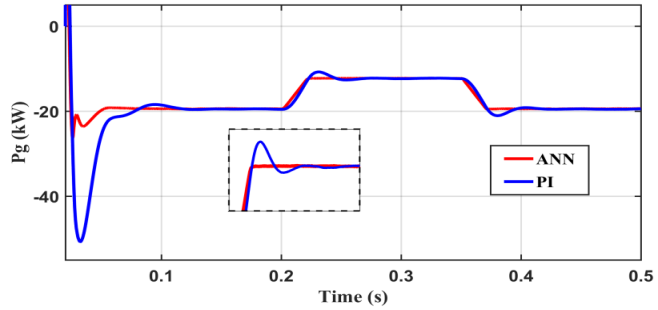

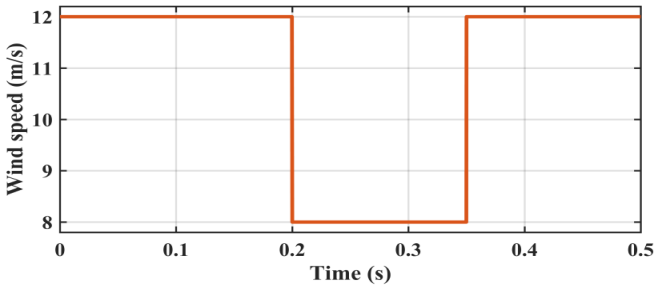

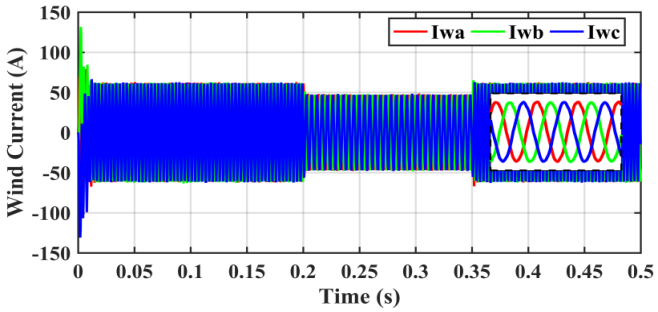

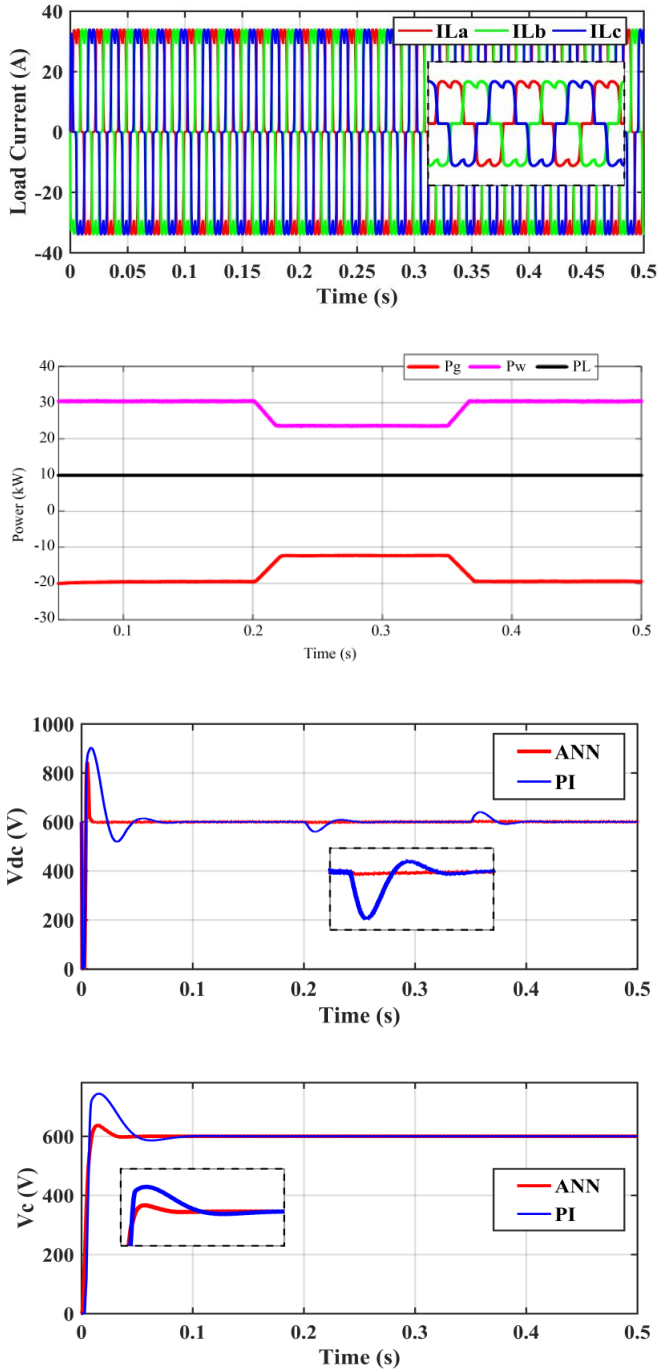

Fig. 15 Simulation results of ANN-Based voltage regulation under wind speed variation

7.2. ANN-Controlled Response under 50% Voltage Sag Condition

Due to the fault condition imposed on the proposed grid-connected wind energy system, there is a voltage sag of approximately 50% in the grid. The grid voltage and the load voltage are then reduced from 230V (nominal) to approximately 100V; the load current will be similarly reduced from 30A to 18A, and the load power will be reduced from 10kW to 2.5kW. The fault induces transient instability and an unbalanced flow of power from the wind generator to the inverter, to the grid. However, due to the inclusion of the adaptive ANN controller within this system, the dynamics of the system were greatly improved. The ANN controller provides compensation for voltage fluctuations via adjustment of the control signals for both the Z-source inverter and the DSTATCOM. The ANN-based controller provided rapid transient recovery and increased damping characteristics of the system, resulting in the rapid return of all system variables to normal after clearing of the sag, as shown in Figure 16. Thus, the proposed control strategy has demonstrated high levels of resiliency and maintained the overall stability of the system during fault-induced voltage sag conditions.

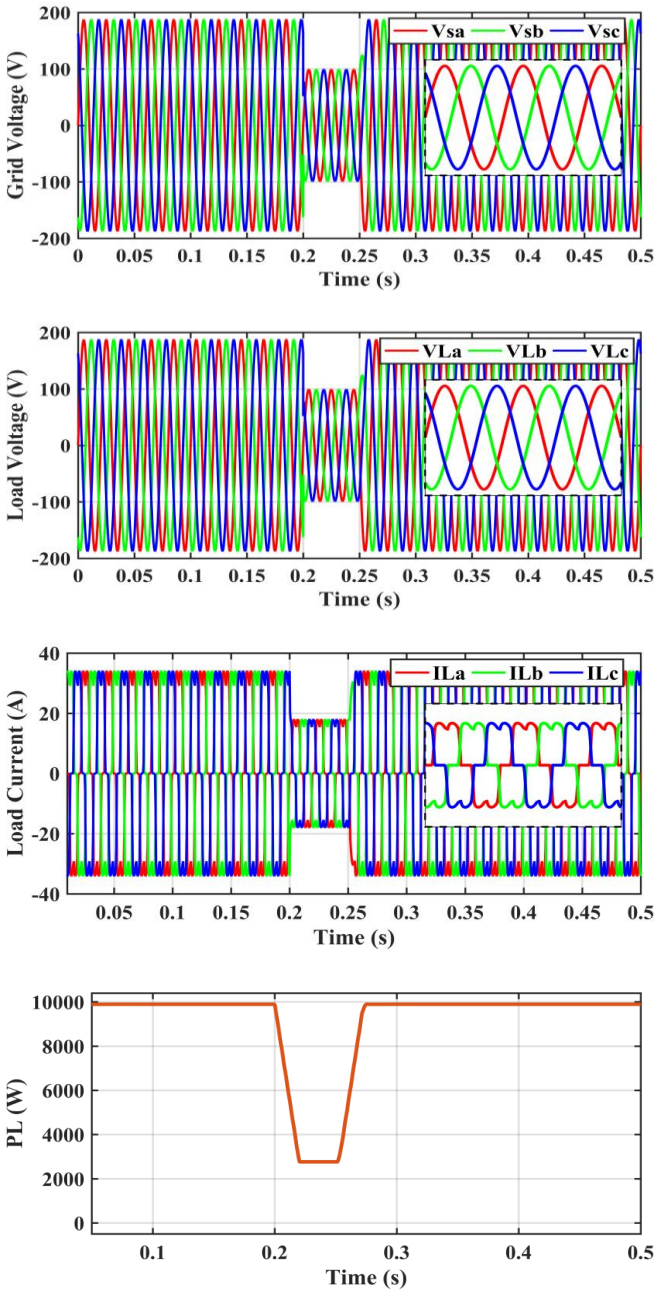

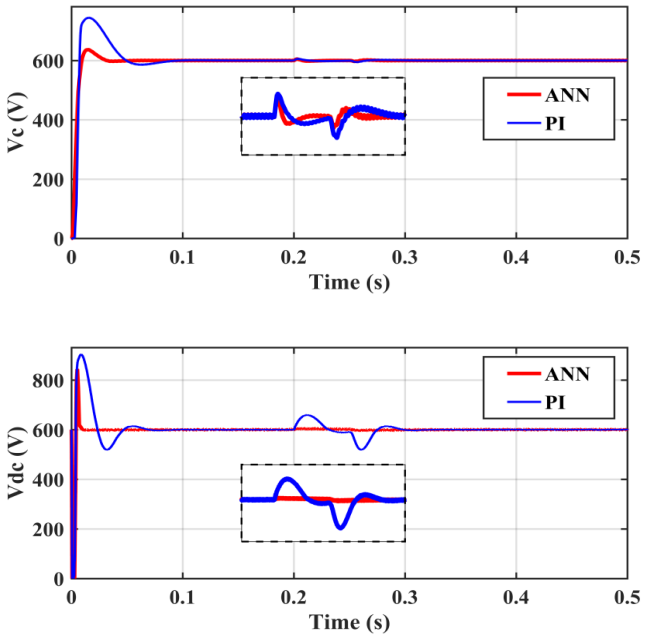

Fig. 16 Simulation results for grid voltage, load voltage, and load current during 50% Voltage sag condition with ANN control.

7.3. Power Quality Performance without DSTATCOM

The PMSG provides the electricity to the utility grid in the proposed grid-connected renewable wind energy system. The power quality of the grid is directly related to the amount of electricity being delivered by the wind generator to the grid. As the level of electricity being produced by the wind generator increases, the grid will have an improved level of voltage stability and less harmonic distortion than when it is producing lower levels of electricity. On the other hand, as the level of electricity being produced by the wind generator decreases, the power quality of the grid also deteriorates.

However, when the wind generator produces large amounts of power under nonlinear load conditions, significant harmonic currents are injected onto the primary distribution lines, thus distorting the waveforms and degrading the power quality of the grid. A DSTATCOM is utilized as a shunt active power filter to reduce the harmonic distortions in the system and to improve the stability of the system, as shown in Figure 17. Simulation studies were performed for two different operating conditions: first, without the DSTATCOM, and second, with the DSTATCOM. In the simulation without the DSTATCOM, when the wind speed was maintained at 12 m/s over the time interval 0-0.2 sec, the total harmonic distortion of the grid current was 12.96%. Additionally, the total harmonic distortion of the load current was 26.58%. Therefore, the presence of nonlinear loads caused significant harmonic distortion of the load current. When the wind speed decreased from 12 m/s - 8 m/s between time intervals of 0.2 sec - 0.35 sec, the total harmonic distortion of the grid current increased to 19.43% due to the unbalance in the power transfer between the wind turbine and the electrical grid as well as the increase in harmonic content of the load current from the nonlinear load as shown in Figure 18. Furthermore, the nonlinear load continued to have a significant harmonic distortion of the load current.

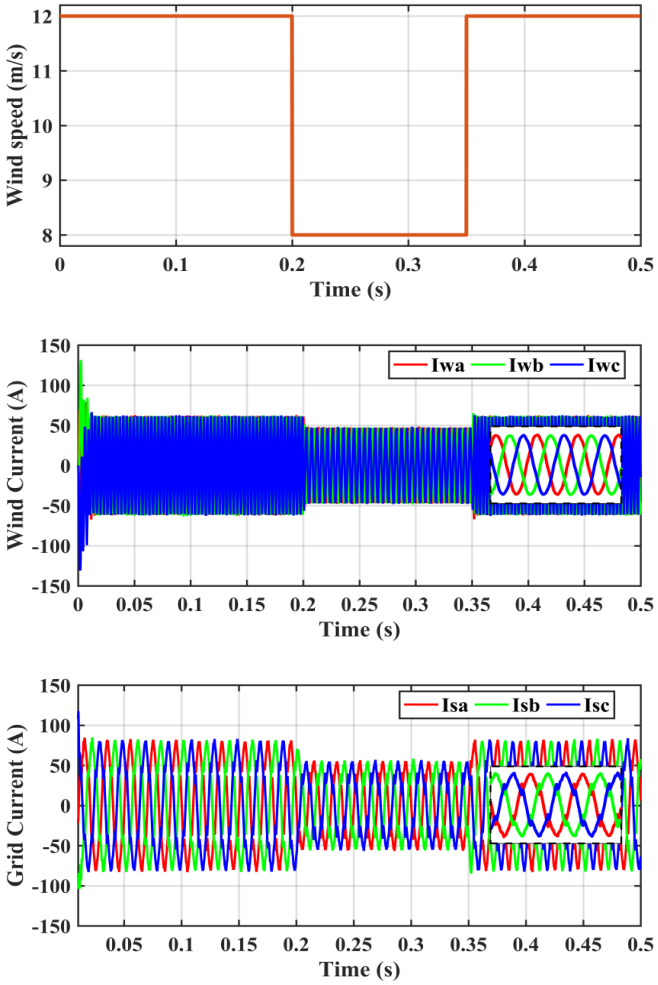

Fig. 17 Simulation results for the power quality performance of grid current without DSTATCOM

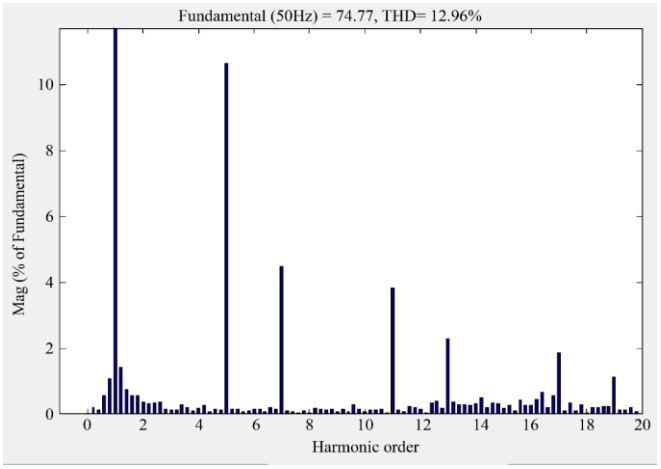

(a)

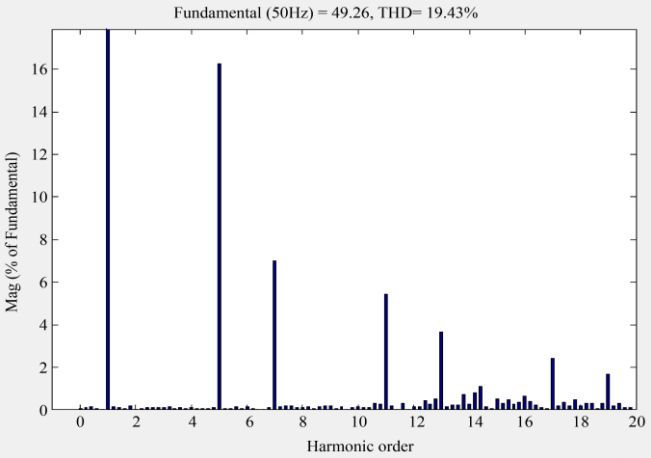

(b)

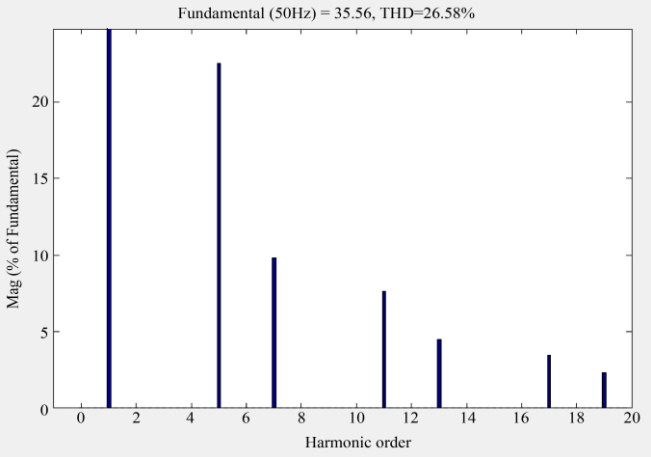

(c)

Fig. 18 Grid Current THD performance without DSTATCOM under wind speeds of (a) 12 m/s, (b) 8 m/s, and (c) Load Current THD.

7.4. Power Quality Performance with DSTATCOM

The DSTATCOM installed with the grid-connected wind energy system provided significantly better power quality than the system without the DSTATCOM, as shown in Figure 15.

The THD for grid currents was only 2.66% when the wind turbine operated at its rated speed of 12 m/s; this indicates that the DSTATCOM was successfully mitigating harmonics introduced into the system at the PCC, as shown in Figure 19.

The THD of the load currents was measured at 26.58% due to the presence of nonlinear loads in the system. With a decrease in wind speed from 12 m/s to 8 m/s, the THD of the grid currents increased slightly to 4.54%, as shown in Figure 20. However, these values are well below the THD limit established in IEEE-519. Therefore, the DSTATCOM effectively prevented the propagation of harmonic distortion introduced from the nonlinear load side into the grid; supported the voltage level; and ensured high-quality grid currents with varying wind speeds and nonlinear loads.

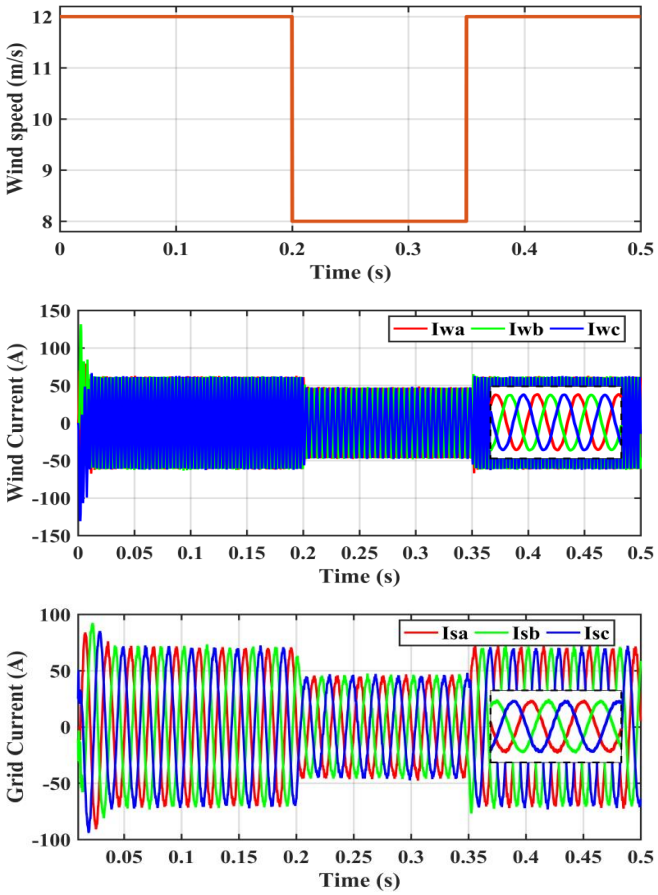

Fig. 19 Simulation results for the power quality performance of grid current with DSTATCOM

Table 2. Comparison of DC-link voltage response using ANN and PI controllers

Parameters	ANN	PI
Rise Time (µs)	5.79	11.055
Settling Time (s)	0.0080	0.0610
Peak Time (s)	0.0051	*0.0088*
Overshoot Time (ms)	40.6926	50.1882
Peak Voltage (V)	843.9345	899.863

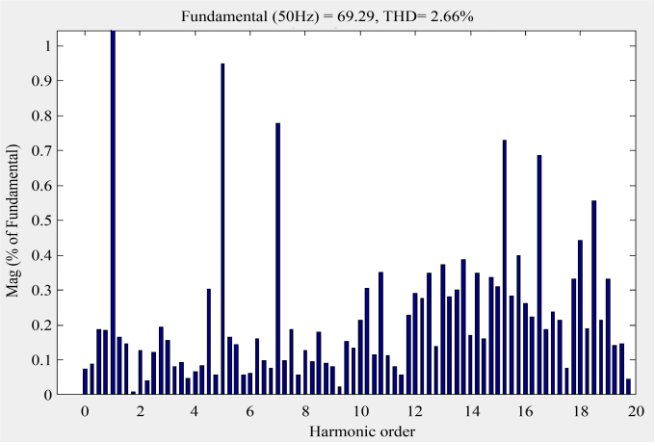

(a)

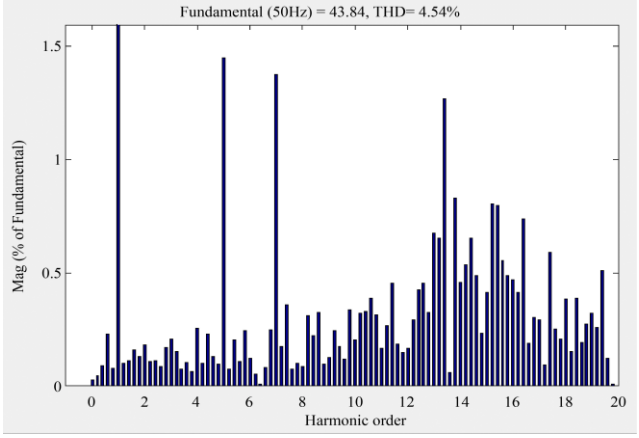

(b)

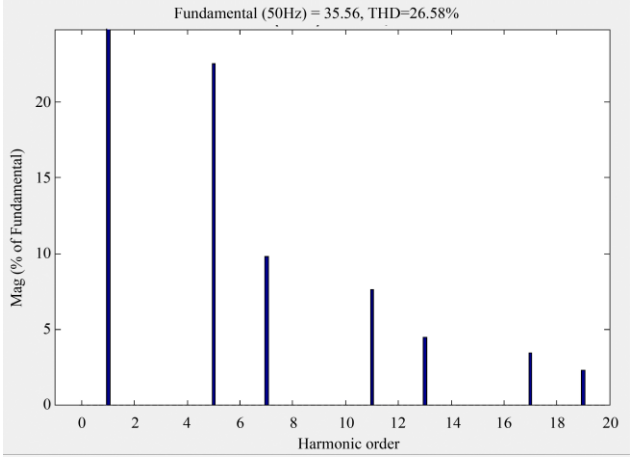

(c)

Fig. 20 Grid current THD performance with DSTATCOM under wind speeds of (a) 12 m/s, (b) 8 m/s, and (c) Load current THD.

8. Conclusion

The proposed ANN-controlled Wind Energy System, utilizing a ZSI and a DSTATCOM, offers better performance in terms of Power Transfer and Quality. Utilizing the ZSI allows for DC-link voltage boosting during AC conversion within one stage, resulting in lower system complexity, lower DC link voltage ripple, and reduced component stress, allowing for efficient power transfer from the PMSG to the grid.

The adaptive ANN controller provides a faster dynamic response than conventional control methods and reduces transients by minimizing oscillation, resulting in faster settling times; thus, it maintains the DC-link voltage and operates smoothly regardless of wind speed and loading variations.

The DSTATCOM is also able to reduce harmonic distortion from nonlinear loads, which results in a reduction of the THD of the grid current from 12.96% at nominal wind speed to 2.65% and from 19.43% at reduced wind speed to 4.54%.

At 50% sag, the system maintains voltage and power levels, limits the impact of the sag on both load current and load power, and returns quickly to normal operating conditions.

The combination of the Z-source inverter, ANN-based control, and DSTATCOM creates a method for providing maximum extraction of power from the wind, provides robust grid support, enhances power quality, and ensures reliable operation of the wind system under both normal and faulted operating conditions.

References

[1] Remus Teodorescu, Marco Liserre, and Pedro Rodríguez, *Grid Converters for Photovoltaic and Wind Power Systems*, Piscataway, NJ, USA: Wiley, 2011. [CrossRef] [Google Scholar] [Publisher Link]

[2] Frede Blaabjerg, Marco Liserre, and Ke Ma, "Power Electronics Converters for Wind Turbine Systems," *IEEE Transactions on Industry Applications*, vol. 48, no. 2, pp. 708-719, 2012. [CrossRef] [Google Scholar] [Publisher Link]

[3] Zhaoqiang Zhang et al., "High-Power Generators for Offshore Wind Turbines," *Energy Procedia*, vol. 35, pp. 52-61, 2013. [CrossRef] [Google Scholar] [Publisher Link]

[4] Zhaoqiang Zhang et al., "State of the Art in Generator Technology for Offshore Wind Energy Conversion Systems," *2011 IEEE International Electric Machines & Drives Conference (IEMDC)*, Niagara Falls, ON, pp. 1131-1136, 2011. [CrossRef] [Google Scholar] [Publisher Link]

[5] Vineet Dahiya, and G. Leena, "Comparative Study of Doubly Fed Induction Generator and Permanent Magnet Synchronous Generator in Wind Energy Conversion System," *International Journal of Electrical Engineering and Technology*, vol. 10, no. 3, pp. 1-7, 2019. [CrossRef] [Google Scholar] [Publisher Link]

[6] Iñaki Arrambide, Itziar Zubia, and Ander Madariaga, "Critical Review of Offshore Wind Turbine Energy Production and Site Potential Assessment," *Electric Power Systems Research*, vol. 167, pp. 39-47, 2019. [CrossRef] [Google Scholar] [Publisher Link]

[7] Lata Gidwani, "A Comparative Power Quality Study of DFIG and PMSG based Wind Energy Conversion System," *WSEAS Transactions on Systems and Control*, vol. 10, pp. 38-47, 2015. [Google Scholar] [Publisher Link]

[8] Seung-Ho Song, Shin-il Kang, and Nyeon-kun Hahm, "Implementation and Control of Grid Connected AC-DC-AC Power Converter for Variable Speed Wind Energy Conversion System," *Eighteenth Annual IEEE Applied Power Electronics Conference and Exposition, 2003. APEC '03*, Miami Beach, FL, USA, vol. 1, pp. 154-158, 2003. [CrossRef] [Google Scholar] [Publisher Link]

[9] M. Chinchilla, Santiago Arnaltes, and Juan Carlos Burgos, "Control of Permanent Magnet Generators Applied to Variable-Speed Wind-Energy Systems Connected to the Grid," *IEEE Transactions on Energy Conversion*, vol. 21, no. 1, pp. 130-135, 2006. [CrossRef] [Google Scholar] [Publisher Link]

[10] Tahar Tafticht et al., "Output Power Maximization of a Permanent Magnet Synchronous Generator based Standalone Wind Turbine," *2006 IEEE International Symposium on Industrial Electronics*, Montreal, QC, Canada, pp. 2412-2416, 2006. [CrossRef] [Google Scholar] [Publisher Link]

[11] Yi Huang et al., "Z -Source Inverter for Residential Photovoltaic Systems," *IEEE Transactions on Power Electronics*, vol. 21, no. 6, pp. 1776-1782, 2006. [CrossRef] [Google Scholar] [Publisher Link]

[12] Miaosen Shen et al., "Comparison of Traditional Inverters and Z-Source Inverter for Fuel Cell Vehicles," *IEEE Transactions on Power Electronics*, vol. 22, no. 4, pp. 1453-1463, 2007. [CrossRef] [Google Scholar] [Publisher Link]

[13] Fang Zheng Peng, "Z-Source Inverter," *IEEE Transactions on Industry Applications*, vol. 39, no. 2, pp. 504-510, 2003. [CrossRef] [Google Scholar] [Publisher Link]

[14] Bhim Singh, Ambrish Chandra, and Kamal Al-Haddad, *Power Quality: Problems and Mitigation Techniques*, John Wiley & Sons, 2014. [CrossRef] [Google Scholar] [Publisher Link]

[15] Sachin Devassy, and Bhim Singh, "Implementation of Solar Photovoltaic System with Universal Active Filtering Capability," *IEEE Transactions on Industry Applications*, vol. 55, no. 4, pp. 3926-3934, 2019. [CrossRef] [Google Scholar] [Publisher Link]

[16] Chandan Kumar, Mahesh K. Mishra, and Marco Liserre, "Design of External Inductor for Improving Performance of Voltage-Controlled DSTATCOM," *IEEE Transactions on Industrial Electronics*, vol. 63, no. 8, pp. 4674-4682, 2016. [CrossRef] [Google Scholar] [Publisher Link]

[17] Salem Rahmani et al., "A Combination of Shunt Hybrid Power Filter and Thyristor-Controlled Reactor for Power Quality," *IEEE Transactions on Industrial Electronics*, vol. 61, no. 5, pp. 2152-2164, 2014. [CrossRef] [Google Scholar] [Publisher Link]

[18] J. Dionísio S. Barros, and J. Fernando Silva, "Multilevel Optimal Predictive Dynamic Voltage Restorer," *IEEE Transactions on Industrial Electronics*, vol. 57, no. 8, pp. 2747-2760, 2010. [CrossRef] [Google Scholar] [Publisher Link]

[19] Mikhail N. Slepchenkov, Keyue Ma Smedley, and Jun Wen, "Hexagram-Converter-based STATCOM for Voltage Support in Fixed-Speed Wind Turbine Generation Systems," *IEEE Transactions on Industrial Electronics*, vol. 58, no. 4, pp. 1120-1131, 2011. [CrossRef] [Google Scholar] [Publisher Link]

[20] Arindam Ghosh, and Gerard Ledwich, *Power Quality Enhancement using Custom Power Devices*, 1st ed., Springer Science, 2012. [Google Scholar] [Publisher Link]

[21] Luís Felipe Normandia Lourenço et al., "Technical Cost of Operating a Photovoltaic Installation as a STATCOM at Nighttime," *IEEE Transactions on Sustainable Energy*, vol. 10, no. 1, pp. 75-81, 2019. [CrossRef] [Google Scholar] [Publisher Link]

[22] Eklas Hossain et al., "Analysis and Mitigation of Power Quality Issues in Distributed Generation Systems using Custom Power Devices," *IEEE Access*, vol. 6, pp. 16816-16833, 2018. [CrossRef] [Google Scholar] [Publisher Link]

[23] Bhim Singh, and Jitendra Solanki, "An Implementation of an Adaptive Control Algorithm for a Three-Phase Shunt Active Filter," *IEEE Transactions on Industrial Electronics*, vol. 56, no. 8, pp. 2811-2820, 2009. [CrossRef] [Google Scholar] [Publisher Link]

[24] Bhim Singh, and Sabha Raj Arya, "Back-Propagation Control Algorithm for Power Quality Improvement using DSTATCOM," *IEEE Transactions on Industrial Electronics*, vol. 61, no. 3, pp. 1204-1212, 2014. [CrossRef] [Google Scholar] [Publisher Link]

[25] Mahesh Kumar Mishra, Arindam Ghosh, and Avinash Joshi, "Operation of a DSTATCOM in Voltage Control Mode," *IEEE Transactions on Power Delivery*, vol. 18, no. 1, pp. 258-264, 2003. [CrossRef] [Google Scholar] [Publisher Link]

[26] Avik Bhattacharya, Chandan Chakraborty, and Subhashish Bhattacharya, "Parallel Connected Shunt Hybrid Active Power Filters Operating at Different Switching Frequencies for Improved Performance," *IEEE Transactions on Industrial Electronics*, vol. 59, no. 11, pp. 4007-4019, 2012. [CrossRef] [Google Scholar] [Publisher Link]

[27] Eknath Borkar, and Nagendra Singh, *Power Quality Enhancement by PV-UPQC for Non-Linear Load*, Artificial Intelligence Techniques in Power Systems Operations and Analysis, 1st ed., Auerbach Publications, pp. 37-64. 2023. [Google Scholar] [Publisher Link]

[28] Amirullah, Ontoseno Penangsang, and Adi Soeprijanto, "High Performance of Unified Power Quality Conditioner and Battery Energy Storage Supplied by Photovoltaic using Artificial Intelligent Controller," *International Review on Modeling and Simulations (IREMOS)*, vol. 11, no. 4, pp. 221-234, 2018. [CrossRef] [Google Scholar] [Publisher Link]

[29] Jayachandran Jayaram, and R. Murali Sachithanandam, "Performance Investigation of Unified Power Quality Conditioner using Artificial Intelligent Controller," *International Review on Modelling and Simulations (IREMOS)*, vol. 8, no. 1, pp. 48-56, 2015. [CrossRef] [Google Scholar] [Publisher Link]

[30] Ramadoni Syahputra, Rama Okta Wiyagi, and Sudarisman, "Performance Analysis of a Wind Turbine with Permanent Magnet Synchronous Generator," *Journal of Theoretical and Applied Information Technology*, vol. 95, no. 9, pp. 1950-1957, 2017. [Google Scholar] [Publisher Link]

[31] Joanne CY Hui, Alireza Bakhshai, and Praveen K. Jain, "An Energy Management Scheme With Power Limit Capability and an Adaptive Maximum Power Point Tracking for Small Standalone PMSG Wind Energy Systems," *IEEE Transactions on Power Electronics*, vol. 31, no. 7, pp. 4861-4875, 2016. [CrossRef] [Google Scholar] [Publisher Link]

[32] Luigi Costanzo, Alessandro Lo Schiavo, and Massimo Vitelli, "Design Guidelines for the Perturb and Observe Technique for Electromagnetic Vibration Energy Harvesters Feeding Bridge Rectifiers," *IEEE Transactions on Industry Applications*, vol. 55, no. 5, pp. 5089-5098, 2019. [CrossRef] [Google Scholar] [Publisher Link]

[33] T. Gowtham Raj, and B. Rajesh Kumar, "Comparative Analysis of Incremental Conductance and Perturb & Observe Mppt Methods for Single-Switch DC/DC Converter," *2018 National Power Engineering Conference (NPEC)*, Madurai, India, pp. 1-5, 2018. [CrossRef] [Google Scholar] [Publisher Link]

[34] Sudheer Vinnakoti, and Venkata Reddy Kota, "ANN based Control Scheme for a Three-Level Converter based Unified Power Quality Conditioner," *Journal of Electrical Systems and Information Technology*, vol. 5, no. 3, pp. 526-541, 2018. [CrossRef] [Google Scholar] [Publisher Link]

[35] Md. Mijanur Rahman et al., "A Comprehensive Study and Performance Analysis of Deep Neural Network-based Approaches in Wind Time-Series Forecasting," *Journal of Reliable Intelligent Environments*, vol. 9, no. 2, pp. 183-200, 2023.[CrossRef] [Google Scholar] [Publisher Link]